Physics – Uspekhi **59** (5) 425 – 445 (2016)

REVIEWS OF TOPICAL PROBLEMS PACS numbers: 42.65.Ky, 42.65.Re, **52.38. – r**

Attosecond electromagnetic pulses: generation, measurement, and application. Generation of high-order harmonics of an intense laser field for attosecond pulse production

V V Strelkov, V T Platonenko, A F Sterzhantov, M Yu Ryabikin

DOI: 10.3367/UFNe.2015.12.037670

Contents

Abstract. This review presents the current state of research on the generation and application of subfemtosecond (or attosecond, where 1 as = 10^{-18} s) ultraviolet and X-ray pulses. Emission of attosecond pulses is closely related to the generation of high-order harmonics in a laser field: the interaction of intense femtosecond laser pulses with matter causes the generation of high-order harmonics whose highest orders range from dozens to thousands and which produce attosecond pulses when they are phase-locked in a sufficiently broad spectral region. Two ways of attosecond pulse generation, the interaction of an intense laser radiation with a gaseous medium and with the edge of a solid state plasma, are discussed. The theory of the microscopic high-frequency response of a gaseous medium to an intense low-frequency laser field is presented together with numerical results based on the solution of the time-dependent Schrödinger equation for an atom in the external field. The review describes the methodology for calculating the macroscopic response and for analyzing the phase-matching in high-order harmonic generation. For the generation of coherent XUV radiation at the edge of a dense plasma, different generation scenarios are discussed, a simple model is proposed, and a comparison of model predictions with numerical results obtained from particle-in-cell (PIC) simulations is given.

Keywords: attosecond pulses, high-order harmonic generation, interaction of intense laser fields with matter, phase matching, time-dependent Schrödinger equation, dense laser plasma, particle-in-cell (PIC) simulations

V V Strelkov Prokhorov General Physics Institute,
Russian Academy of Sciences,
ul. Vavilova 38, 119991 Moscow, Russian Federation;
Moscow Institute of Physics and Technology (State University),
Institutskii per. 9, 141700 Dolgoprudnyi, Moscow region,
Russian Federation
E-mail: strelkov.v@gmail.com
V T Platonenko, A F Sterzhantov Lomonosov Moscow State University,
Leninskie gory 1, 119991 Moscow, Russian Federation
M Yu Ryabikin Institute of Applied Physics,
Russian Academy of Sciences,
ul. Ul'yanova 46, 603950 Nizhny Novgorod, Russian Federation;
Lobachevsky State University of Nizhny Novgorod,
prosp. Gagarina 23, 603950 Nizhny Novgorod, Russian Federation

Received 7 September 2015, revised 1 December 2015
Uspekhi Fizicheskikh Nauk **186** (5) 449 – 470 (2016)
DOI: 10.3367/UFNr.2015.12.037670
Translated by M Yu Ryabikin; edited by A Radzig

1. Introduction

Since the advent of lasers, the development of nonlinear optics has been closely related to the progress in laser pulse shortening. State-of-the-art laser systems have been demonstrated furnishing an opportunity to produce femtosecond pulses whose duration is comparable to the light cycle (one oscillation period for a Ti:sapphire laser is about 2.7 fs). Hence, it is impossible to further reduce the duration of light pulses with the carrier wavelength located in the visible region of the electromagnetic spectrum. In contrast, ultraviolet or shorter-wavelength subfemtosecond pulses are within reach. This review presents the current status of research in the field of generation and application of subfemtosecond (or attosecond, where 1 as = 10^{-18} s) pulses in the UV and X-ray spectral ranges.

The prevalent approach to the production of attosecond pulses is closely related to the generation of high-order harmonics of a laser field: the interaction of intense femtosecond laser pulses with matter causes the generation

of high-order harmonics (high-order harmonic generation, HHG), whose highest orders, depending on the specific conditions, can range from dozens to thousands. As was experimentally demonstrated in the early 2000s, under certain conditions the harmonics can be phase-locked so that they are added up constructively to form a train of attosecond pulses in the UV or X-ray region. As the shortest of the electromagnetic pulses produced to date, these pulses provide a unique tool for the direct measurement of attosecond dynamics of processes important for various branches of physics, chemistry, biology, applied sciences, etc., which determines the relevance of this subject.

The layout of the paper is as follows.Two ways of attosecond pulse generation, the interaction of an intense laser field with a gaseous medium and with the edge of a solid state plasma, are discussed in this review.

In the first of these areas, significant advances have been achieved in both the experimental implementation and the theoretical description of the phenomenon. In Section 2, along with a review of recent experimental data related to HHG in gases, we present theoretical approaches to the description of coherent ultraviolet light generation via HHG in a gaseous medium exposed to an intense low-frequency elliptically polarized laser field of arbitrary ellipticity. A calculation of both the microscopic and macroscopic responses is discussed. The quantum-mechanical theoretical approaches presented here, which are based on a semiclassical description of the electron motion, are applicable, strictly speaking, only to the tunneling regime (i.e., to those cases where the Keldysh parameter γ [1] is much less than unity). However, a comparison with the numerical results and experimental data shows that the theory is also valid at $\gamma \approx 1$.

In Section 3, we analyze the prospects for the production of attosecond pulses in the interaction of intense laser radiation with a dense plasma. The calculated results exhibit that, when a laser pulse of relativistic intensity is reflected off the edge of a solid target or passes through a thin foil, atto- or subattosecond pulses are generated, whose generation efficiency can be very high under certain conditions. Prospects for the experimental implementation of this technique for attosecond pulse generation are also considered.

2. Attosecond pulse generation in gases. Mechanism of the phenomenon and its theoretical description

2.1 Conditions for attosecond pulse production. Semiclassical theory of the high-order harmonic generation process

As mentioned in the Introduction, attosecond pulse production requires the use of coherent light in the ultraviolet (UV) or X-ray regions of the spectrum. Recently, significant progress has been achieved in the development of free-electron lasers (FELs) operating in these spectral regions [2–5]. However, FELs are usually characterized by a huge size and costliness, as well as by a low degree of temporal coherence of the generated pulses [6]. Although the last problem is solved to a large extent by seeding FELs with external coherent light (in particular, the use of seed light produced by HHG in gases driven by femtosecond lasers has been demonstrated [7, 8]), FELs cannot yet be regarded as practical tools for extensive experimental research in attosecond physics. The most significant advancements in attosecond pulse generation are due to the other way of producing coherent high-frequency light, namely, with HHG in gaseous media. This effect was first observed experimentally in the late 1980s and early 1990s [9–16]. The early experimental work in this field was reviewed in Refs [17, 18]. Progress in experimental techniques made it possible to produce coherent light of ever higher frequencies by this method. In particular, HHG sources were extended by the late 1990s into the 'water window' region [19, 20], important for biochemical and other research (the range of wavelengths between 2.3 and 4.4 nm, or photon energies between 284 and 543 eV, where the carbon-containing biological substrates efficiently absorb radiation, whereas water is relatively transparent); furthermore, in 2005, high-order harmonic emission at a wavelength of 1 nm (corresponding to a photon energy of about 1.3 keV) was demonstrated [21].

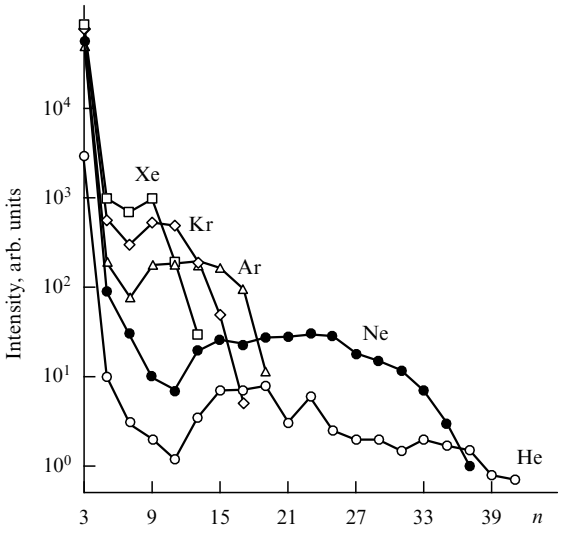

Figure 1. Typical spectra of harmonic generation by intense linearly polarized laser light in a gas. Shown are the intensities I_n of harmonics generated in He, Ne, Ar, Kr, and Xe driven by a dye laser ($\lambda = 0.616$ μm) with intensities of 1.4, 1.9, 1.9, 1.5, and 2.0×10^{14} W cm^{-2} for He, Ne, Ar, Kr, and Xe, respectively. (Taken from Ref. [14].)

It should be noted that, as far back as the 1960s, HHG in plasmas was studied theoretically [22] (see also Ref. [23]). Presumably, HHG from bulk plasma was observed for the first time in study [24]. However, this mechanism has not been studied experimentally in detail, since it usually has a relatively low efficiency. More actively studied is HHG from solid-density plasma surfaces (see reviews [25, 26]). This method is promising in terms of high-intensity attosecond pulse generation. In experiments implementing this approach, the generation of X-rays was demonstrated with photon energies exceeding those of the incident light by a factor of a few thousand [27]. Recent experiments have revealed that high-order harmonics emitted from a plasma surface are phase-locked [28, 29]; furthermore, direct experimental evidence was reported recently that these harmonics constitute a train of pulses, each of duration much shorter than the oscillation period of the incident light [30].

In the spectrum of high-order harmonics generated in a gas, a fast decrease in intensity versus harmonic order in the low-frequency region is followed by a broad plateau-like distribution that extends to the high-frequency region and then ends in an abrupt cutoff (Fig. 1). As a result of numerical

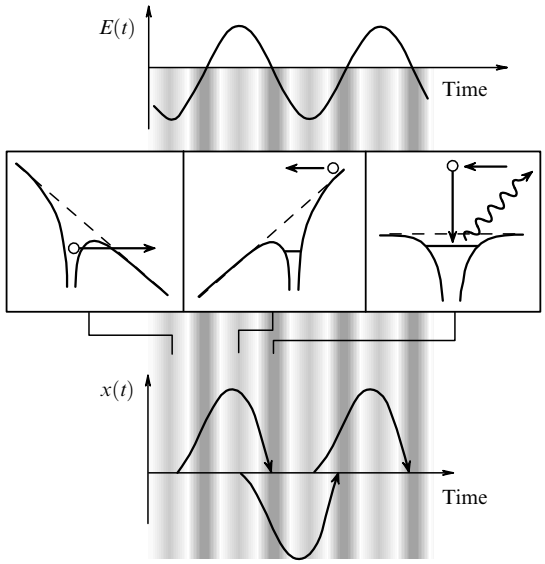

Figure 2. Explanation of the three-step mechanism for the generation of high-order harmonics of intense laser light in a gas.

calculations [31], the empirical law for the cutoff position was found, which agrees well with numerous experimental data:

$$N_{\max} \approx \frac{I_p + 3U}{\omega_0}, \quad (1)$$

where I_p is the ionization potential of the atom, and $U = E_0^2/(4\omega_0^2)$ is the average energy of electron oscillations in an AC electric field of amplitude E_0 and frequency ω_0 (hereinafter, atomic units, $e = m_e = \hbar = 1$, are used for convenience).

The low-frequency region of the harmonic spectrum, showing a rapid decrease in intensity with the harmonic order, is mostly due to the nonlinearity of the intraatomic response, similar to what takes place in harmonic generation at low driving intensities. The boundary of this region is determined by the maximum frequency attributable to the electron motion inside an atom, i.e., by the ionization potential. A decisive role in understanding the mechanism of the generation of higher-order harmonics, as well as in explaining a number of other nonlinear processes associated with atomic ionization in an intense laser field, has been played by a so-called semiclassical model introduced in Refs [32, 33] (some similar considerations appeared earlier in Refs [34–36]). According to the semiclassical model, HHG proceeds basically as a three-step process in which the elementary acts (Fig. 2) are: (i) ejection of electron from an atom via tunneling ionization; (ii) its acceleration by the optical field which pushes the electron first away from the parent ion and then back toward it as the field changes sign, and (iii) the recollision of the electron with the parent ion, which may result in high-energy photon emission.

The maximum energy of the photon emitted during this process is determined by the maximum kinetic energy $E_{\max}$ that the electron can gain before the recollision event. As a result of recollision with the ion, the electron can recombine into the atomic ground state to emit a photon with the energy equal to $\omega_{\max} = I_p + E_{\max}$.

Let us assume that the field $E(t) = E_0 \sin(\omega_0 t)$ is linearly polarized along the x-axis. Since the radius of electron oscillations in a strong field far exceeds the atomic size (for a

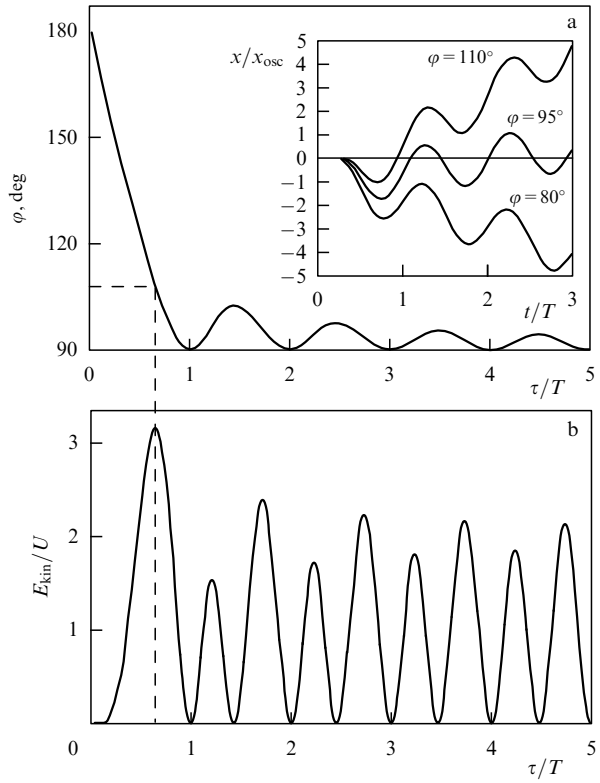

Figure 3. (a) Phase of the laser field at the instant of electron release vs. the time of electron excursion prior to its returning to the parent ion. Inset: electron trajectories launched at various phases of the field; depending on this phase, the electron either never returns to the parent ion or revisits it at least once. (b) Kinetic energy gained by returning electron vs. its excursion time.

driving field with a wavelength of 800 nm and intensity on the order of 10^{14} W cm^{-2}, the oscillation radius $x_{\text{osc}} = E_0/\omega_0^2$ reaches a few dozen Bohr radii), the effect of the Coulomb field of the ion on the electron motion can be ignored.

In what follows, we will assume that, as a result of ionization, an electron initially bound in the atom undergoes a transition into the continuum at some instant t_i, starting its free motion from the origin with a zero initial velocity. By solving Newton's equation, we find that the ejected electron trajectories launched at the phases $\varphi = \omega_0 t_i$ of the laser field in the intervals $0 \leqslant \varphi \leqslant \pi/2$, $\pi \leqslant \varphi \leqslant 3\pi/2$, etc., never come back to the parent ion, whereas the electrons born in the intervals $\pi/2 \leqslant \varphi \leqslant \pi$, $3\pi/2 \leqslant \varphi \leqslant 2\pi$, etc., may revisit the parent ion once or several times (see inset to Fig. 3a).

One can find from the solution of Newton's equation [17, 37] that the electron's return time t_r is related to its excursion time

$$\tau = t_r - t_i \quad (2)$$

according to the condition

$$\tan\varphi = \frac{\omega_0\tau - \sin(\omega_0\tau)}{\cos(\omega_0\tau) - 1}, \quad (3)$$

while the kinetic energy gained by the returning electron is expressed as

$$E_{\text{kin}} = 2U\,\frac{C^2(\omega_0\tau)\omega_0\tau}{\omega_0\tau - \sin(\omega_0\tau) - C(\omega_0\tau)}, \quad (4)$$

where $C(\omega_0\tau) = \sin(\omega_0\tau) - 2[1 - \cos(\omega_0\tau)]/(\omega_0\tau)$.

Notice that the instants t_i^m of atomic ionization for the case of a nonmonochromatic (two-color) laser field can be found using a convenient graphical method developed by Paulus et al. [38].

As follows from an analysis of formulas (3) and (4), the electron's return kinetic energy E_{kin} passes a maximum value of $E_{max} \approx 3.17U$ (see Fig. 3b) corresponding to $\varphi = 1.88$ (108°), $\omega_0\tau = 4.09$ (234°), and $\omega t_r = 5.97$ (342°). Hence, we obtain a formula for the harmonic order corresponding to the high-frequency cutoff of the spectrum plateau:

$$N_{max} = \frac{I_p + 3.17U}{\omega_0}\,, \tag{5}$$

which agrees well with empirical formula (1).

Electron trajectories corresponding to atomic ionization at the laser phase in the interval of $108° < \varphi < 180°$ and, hence, the excursion time within $0 < \tau < 0.65\,T$, where T is the oscillation period of the driving field, are called 'short', whereas all other trajectories are called 'long'. As can be seen in Fig. 3, each value of the return kinetic energy within $2.4U < E_{kin} < 3.17U$ corresponds to only two trajectories (one short and one long), whereas for lower energies there is a greater number of return trajectories. This means that up to harmonic orders corresponding to approx. 3/4 the width of the plateau, the electron trajectories with $\tau > T$, i.e., with multiple returns to the parent ion, contribute to the harmonic signal. Notice, however, that, as the quantum-mechanical treatment indicates (see below), the contribution of these trajectories decreases significantly with increasing τ, because of the spreading of the electron wave packet.

In a periodically oscillating field, the three-step process described above occurs over and over with a certain probability every half-cycle of the driving field (see the lower part of Fig. 2). This leads to the fact that the emitted spectrum consists of a set of harmonics separated by $2\omega_0$. Due to the isotropy of a gaseous medium, only odd harmonics are emitted.

Thus, HHG in gases turns out to be useful for producing attosecond pulses, since the emission spectrum in this case contains a wide area (plateau) of harmonics having similar intensities. If these spectral components are perfectly phase-locked, the duration of a pulse made up of them is determined by the inverse spectral width of this area. Specifically, a signal obtained by superposing q phased odd-order harmonics is a periodic sequence of pulses, each of duration $T/(2q)$, with the repetition period $T/2$ [34, 39]. The question of high-order harmonic synchronization is addressed in Section 2.2.

2.2 Quantum-mechanical description of the high-order harmonic generation process. Numerical calculations

The polarization of a medium volume element, defined as the dipole moment per unit volume, is $\mathbf{P}(t) = N\boldsymbol{\mu}(t)$, where N is the concentration of atoms or molecules, and $\boldsymbol{\mu}$ is the quantum-mechanical average of the dipole moment defined as

$$\boldsymbol{\mu}(t) = \langle \psi(\mathbf{r}, t) | -\mathbf{r} | \psi(\mathbf{r}, t) \rangle\,, \tag{6}$$

where $\psi(\mathbf{r}, t)$ is the electron wave function. For simplicity, we will hereinafter be limited to the case of a one-electron atom. The single-active-electron approximation [31, 40] is often also used for multielectron atoms; in this case, it is assumed that the interaction of an atom with the external field is governed solely by the electron on the highest occupied energy level, which is most weakly bound to the nucleus, whereas the other electrons are considered to be frozen inside the atom and constitute, together with the nucleus, a particle whose interaction with the active electron is described by the effective potential $V(\mathbf{r})$.

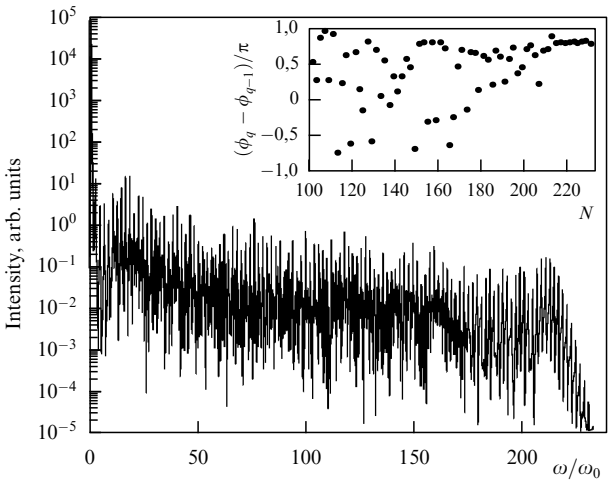

Figure 4. Harmonic spectrum calculated numerically for a hydrogen atom driven by a trapezoidal linearly polarized laser pulse with a wavelength of 1600 nm, peak intensity of 2×10^{14} W cm^{-2}, and duration of 18 optical cycles. Inset: phase difference $\varphi_q - \varphi_{q-1}$ between the neighboring odd harmonics vs. the harmonic order $N = 2q + 1$.

To describe the interaction of an atom with the laser field, we will apply the electric dipole approximation. The electron wave function can then be found by solving the time-dependent Schrödinger equation

$$\mathrm{i}\,\frac{\partial}{\partial t}\,|\psi(\mathbf{r}, t)\rangle = \left(-\frac{1}{2}\,\nabla^2 + V(\mathbf{r}) + \mathbf{r}\mathbf{E}(t)\right)|\psi(\mathbf{r}, t)\rangle\,. \tag{7}$$

In general, equation (7) can only be solved numerically (see, e.g., Refs [32, 40–46] for numerical methods). The example illustrated in Fig. 4 represents the numerical results for the high-order harmonic spectrum obtained using the split-operator fast Fourier transform method (see Refs [47, 48] for details of the calculations; the numerical method was proposed by Fleck et al. [49]). The spectrum possesses a pronounced plateau-like distribution with a high-frequency cutoff whose position agrees well with that given by the classical analysis [see formula (5), which gives $N_{max} \approx 213$ when applied to the same case as in Fig. 4].

The inset to Fig. 4 gives the numerical results for the phase difference between two adjacent odd harmonics as a function of the harmonic order. The harmonic phase distribution seems to be random, which, at first glance, points to the impossibility of obtaining short pulses by superposing several neighboring harmonics. This, however, is not actually the case. As an example, the time profile of the total signal in the frequency window between the 171st and 191st harmonics is plotted in Fig. 5a. It is seen that the time-dependent harmonic signal exhibits two dominant peaks (labelled *1* and *2* in Fig. 5) per half cycle. As we move the spectral window further towards higher frequencies, every pair of peaks converges and finally merges into a single peak for the harmonics in the plateau cutoff region.

The time–frequency evolution of the harmonic signal described above is clearly illustrated by the wavelet scalo-

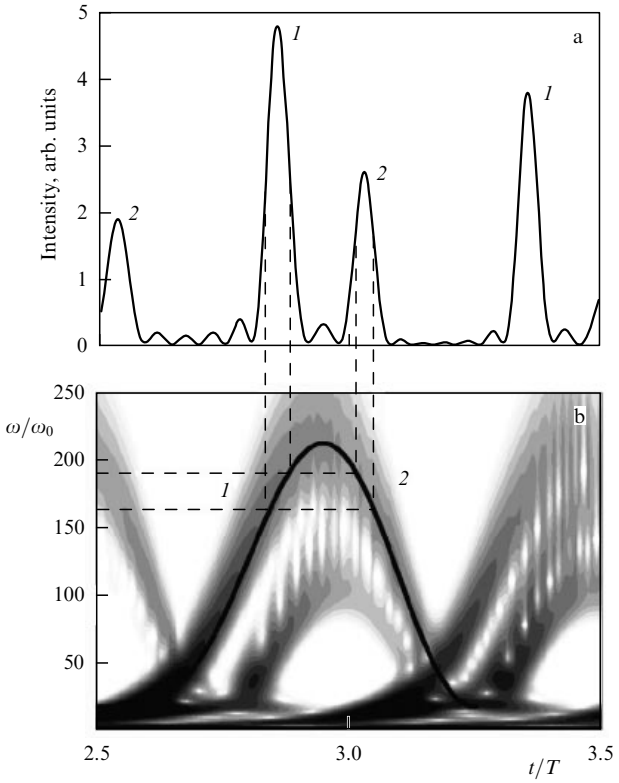

Figure 5. (a) Time profile of the harmonic signal in the frequency window of the 171th to 191th harmonics. The parameters of the laser pulse are the same as in Fig. 4. (b) Detail of the scalogram of the wavelet transform of the harmonic signal whose spectrum is shown in Fig. 4. The solid line depicts the result obtained from the analysis of the electron's classical motion (see text). (Taken from Ref. [50].)

gram displayed in Fig. 5b (see Ref. [51] for details of the wavelet transform). The solid line in Fig. 5b shows the time dependence of $(E_{\rm kin}(t) + I_{\rm p})/\omega_0$, where $E_{\rm kin}$ is given by the classical formula (4) with $t = t_{\rm r}$. Good agreement between the quantum-mechanical and classical treatments of the high-order harmonic generation process is seen: the time–frequency structure of the generated harmonic signal contains alternating areas with positive and negative chirp (the areas labelled, respectively, *1* and *2* in Fig. 5b), consistent with the analogous rise and fall features of the electron's return kinetic energy as a function of time. Trajectories contributing to the areas *1* and *2* in Fig. 5b are called, respectively, 'short' and 'long', as mentioned above. Notice that the time–frequency structure of the harmonic signal at low ω is complicated due to the contribution from even longer trajectories (lasting longer than the laser oscillation period) supporting electron multiple returns to the parent ion. However, with increasing electron excursion time in the continuum, the contribution of such trajectories compared to the contribution of shorter paths is reduced due to the quantum-mechanical spreading of the electron wave packet (see Section 2.3).

The complex behavior of the harmonic phases in the low-frequency part of the plateau in Fig. 4 results from interference between the contributions of different electron trajectories. As the harmonic frequency increases, the properties of these contributions become more similar and, eventually, for harmonics near the high-frequency cutoff, these contributions are merged into one, which is manifested in the regular behavior of the harmonic phases.

2.3 Quantum-mechanical description of the high-order harmonic generation process. Analytical theories

Under certain assumptions, the construction of analytical or semianalytical theories is feasible (see, e.g., Refs [52–60]), allowing the theoretical study of the HHG process without resorting to the numerical solution of the Schrödinger equation. We begin with a brief description of a widely used theory developed by Lewenstein et al. [52].

The wave function in formula (6) can be represented as the sum of terms corresponding to the bound and free electron: $\psi = \psi_{\rm b} + \psi_{\rm f}$. We then have

$$\boldsymbol{\mu} = \langle\psi_{\rm b}|-\mathbf{r}|\psi_{\rm b}\rangle + \langle\psi_{\rm b}|-\mathbf{r}|\psi_{\rm f}\rangle + \langle\psi_{\rm f}|-\mathbf{r}|\psi_{\rm b}\rangle + \langle\psi_{\rm f}|-\mathbf{r}|\psi_{\rm f}\rangle\,. \tag{8}$$

The first term on the right-hand side of formula (8) corresponds to the contribution to the dipole moment caused by bound–bound transitions; the second and third terms define the contributions of free–bound transitions, and, finally, the last term corresponds to free–free transitions. The first term, which describes the intraatomic transitions, is responsible for the sharply falling low-frequency part of the harmonic spectrum and does not play a significant role in respect to the generation of attosecond pulses (APs). In a typical case of weak ionization, the contribution of the last term in formula (8) to the dipole moment is relatively small and, as a rule, is not taken into account (the opposite case is considered in Refs [53, 58, 61]). Accordingly, the HHG theories are usually focused on free–bound electron transitions. The theory developed by Lewenstein et al. [52] also ignores the contribution of the intermediate bound states, which is justified for HHG at commonly used driving field intensities ($I \sim 10^{14}-10^{15}$ W cm^{-2}), at which tunneling ionization occurs [1]. The wave function is represented as a superposition of the atomic ground state $|0\rangle$ and the integral over the set of continuum states $|\mathbf{v}\rangle$ ($\mathbf{v}$ is the electron velocity in the continuum):

$$\big|\psi(\mathbf{r},t)\big\rangle = \exp\left(\mathrm{i}I_{\rm p}t\right)\left(a(t)|0\rangle + \int b(\mathbf{v},t)|\mathbf{v}\rangle\,\mathrm{d}^3\mathbf{v}\right). \tag{9}$$

The influence of the Coulomb field of the nucleus on the electron motion in the continuum is disregarded, just as in the semiclassical theory discussed above. Since the case of weak ionization is considered, the change in amplitude of the ground state wave function is assumed to be negligible: $a(t) \approx 1$. Substituting Eqn (9) into Eqns (6) and (7) and making some transformations, we obtain the following expression for the dipole moment

$$\boldsymbol{\mu}(t) = \mathrm{i}\int_0^t \mathrm{d}t' \int \mathrm{d}^3\mathbf{p}\left[\mathbf{E}(t')\,\mathbf{d}\left(\mathbf{p} - \frac{1}{c}\,\mathbf{A}(t')\right)\right] \times \exp\left(-\mathrm{i}S(\mathbf{p},t,t')\right)\mathbf{d}^*\left(\mathbf{p} - \frac{1}{c}\,\mathbf{A}(t)\right) + \text{c.c.} \tag{10}$$

Here, $\mathbf{p} = \mathbf{v} + (1/c)\mathbf{A}(t)$ is the canonical momentum, $\mathbf{A}(t)$ is the vector potential of the laser field, $\mathbf{d}(\mathbf{v}) = \langle\mathbf{v}|\mathbf{r}|0\rangle$ is the transition dipole moment between the bound state and the continuum state of the electron, and $S(\mathbf{p},t,t')$ is the semiclassical action which defines the phase accumulated by the electron wave function during propagation between the instants t' and t:

$$S(\mathbf{p},t,t') = \int_{t'}^{t} \mathrm{d}t''\left[\frac{\left(\mathbf{p} - (1/c)\mathbf{A}(t'')\right)^2}{2} + I_{\rm p}\right]. \tag{11}$$

The main contribution to the integral over $\mathbf{p}$ in formula (10) comes from the stationary points of the semiclassical action: $\nabla_{\mathbf{p}} S(\mathbf{p}, t, t') = 0$ [52]. The presence of stationary points greatly simplifies the calculation of this integral, allowing, with the help of the stationary phase method, it to be reduced to a single integral over the time variable (for brevity, the final expression is omitted here; see Ref. [52] for details). On the other hand, from formula (11) it can easily be seen that $\nabla_{\mathbf{p}} S(\mathbf{p}, t, t')$ is the difference between the electron coordinates at the instants t' and t: $\nabla_{\mathbf{p}} S(\mathbf{p}, t, t') = \mathbf{e}_x(x(t) - x(t'))$. Therefore, it can be concluded that the greatest contribution to the harmonic emission comes from the electrons that tunnel away from the atom and later come back to the same position when moving in an oscillating electric field. Further application of the stationary phase method (when integrating over the time variable $\tau = t - t'$) reveals that the stationary point of the semiclassical action with respect to τ corresponds to the zero value of the electron's initial velocity.

Thus, the quantum theory [52] confirms the basic assumptions of the semiclassical model presented above (allowing, moreover, a systematic consideration of the role of a number of purely quantum-mechanical phenomena, such as tunneling, electron wave-packet diffusion, and quantum interference). We emphasize, in particular, that the quantum-mechanical approach allows us to consider the synchronization of the generated harmonics.

To find the spectrum of the dipole moment $\boldsymbol{\mu}(t)$, one can again apply the stationary phase method. It turns out that the stationary points of the rapidly oscillating phase factor of the integrand in the expression for the Fourier transform of the dipole moment at the frequency of the Nth-order harmonic correspond to those instants t_N of time at which the kinetic energy of a classical electron returning to the ion is equal to $E_{\text{kin}} = N\omega_0 - I_{\text{p}}$. In agreement with the numerical results presented in Fig. 5, theory [52] predicts that for sufficiently high harmonics the dipole moment is for the most part determined by only two trajectories (corresponding to τ_1 and τ_2). The contribution of the sth trajectory ($s = 1, 2$) to the component of the dipole moment at frequency $N\omega_0$ in this case is characterized by the phase difference $\Phi_{N,s} = S(t_{N,s}) - N\omega_0 t_{N,s}$ between the dipole moment and the pump wave (where $S(t_{N,s})$ is the value of the semiclassical action corresponding to the electron trajectory with the return time $t_{N,s}$).

Action (11) and, hence, the harmonic phase depend on the laser radiation intensity I. Because of the spatial variations of I in the laser beam, the phase of the dipole moment is generally different for different atoms in the interaction volume, so the function $\Phi(I)$ is an important characteristic affecting the coherence of the harmonic field accumulated at the output of the medium. Similarly, changes in the instantaneous laser radiation intensity with time may degrade, due to the dependence $\Phi(I)$, the temporal coherence of the harmonic field. Detailed quantum-mechanical calculations [62–64] allow us to conclude that for both electron trajectories making the main contribution to the harmonic signal, the dependence $\Phi(I)$ is approximately linear:

$$\Phi_s(I) \approx -\alpha_s I, \tag{12}$$

but the proportionality coefficient for the long path is many times greater in magnitude than that for the short path: $|\alpha_2| \gg |\alpha_1|$. This fact is very important in the context of the selection of the contributions from appropriate trajectories to the harmonic signal (see Section 2.4).

Just as in Ref. [52], the versions of the quantum-mechanical theory developed in Refs [17, 55, 65–67] can be linked to the semiclassical model of HHG by applying the stationary phase method to the integrals describing the response of an atom to an external field: the solutions for the stationary phase (quantum trajectories or quantum orbits) correspond approximately to the electron trajectories in the classical model. The atomic response at each harmonic frequency is composed of several terms corresponding to different quantum trajectories that lead from the initial to the final state. The role of these trajectories in HHG, above threshold ionization, and electron rescattering by the parent ion was first discussed in the early theoretical studies by Lewenstein et al. [52, 68] and Becker et al. [65], and has been studied in detail in Refs [69–74] (see also review [37]). Strictly speaking, the use of quantum trajectories ensures a good approximation only in the tunneling limit. The applicability of this approximation to the cases of intense laser pulses with realistic parameters (which do not always strictly satisfy the condition $\gamma \ll 1$) has been addressed by Bauer et al. [75, 76] by comparing the theoretical predictions with the results of direct numerical solution to the Schrödinger equation.

Using the quantum orbit approach, Ivanov et al. [77] and Platonenko [56, 57] developed alternative versions of the HHG theory, in which the amplitude of the microscopic response is represented as the product of the factors responsible for atomic ionization, free-electron wave-packet propagation under the influence of the laser field, and emission of a high-frequency photon. This representation has allowed the approximate account for the effect of Coulomb attraction to the ion core on the electron wave-packet motion. In study [78], theory [56] has been generalized to the case of an elliptically polarized field.

Below, we will describe in more detail theory [78], which is based on the semiclassical treatment of electron motion along the major axis of the polarization ellipse of the laser field after ionization. The electron motion in a plane perpendicular to this axis is described fully quantum-mechanically. The theory makes use of the ionization rate calculated via the numerical integration of the Schrödinger equation for a one-electron model of the atom in the laser field. In addition, the theory takes into account the attraction of a free-electron wave packet to the parent ion immediately after ionization (through the introduction of the adjustable parameter δ optimized by comparison with the numerical results), as well as the attraction of the returning electron wave packet to the parent ion.

This theory allows us to calculate separately the contributions of different quantum trajectories to HHG. The dependence of the characteristics of these contributions on the parameters of the driving field turns out to be much simpler than that for a full harmonic signal.

Below, the final expressions are given, which define the single-atom response obtained through the use of this theory.

The electron microscopic response to the laser field action is determined by the second derivative of the dipole moment (6). In accordance with Ehrenfest's theorem, it is equal to the quantum-mechanical mean value of the force acting on the electron:

$$\ddot{\boldsymbol{\mu}}(t) = \mathbf{f}_{\text{full}}(t)\,,$$

where

$$\mathbf{f}_{\text{full}}(t) = -\left\langle \psi(\mathbf{r},t)\middle|\mathbf{E}(t) + \frac{\mathbf{r}}{r^3}\middle|\psi(\mathbf{r},t)\right\rangle . \tag{13}$$

What will be calculated below is just the quantum-mechanical average of the force, rather than of the dipole moment. It is evident that in the dipole approximation the first term on the right-hand side of expression (13), namely

$$\langle\psi(\mathbf{r},t)|\mathbf{E}(t)|\psi(\mathbf{r},t)\rangle = \mathbf{E}(t)\langle\psi(\mathbf{r},t)|\psi(\mathbf{r},t)\rangle = \mathbf{E}(t)\,,$$

does not contain high-frequency oscillations responsible for the generation of UV radiation. Therefore, we consider below only the second term

$$\mathbf{f}(t) = -\left\langle \psi\middle|\frac{\mathbf{r}}{r^3}\middle|\psi\right\rangle . \tag{14}$$

The following expression for this quantity was obtained in Ref. [78]:

$$\mathbf{f} = \sum_m \{f_x, f_y, 0\}\,, \tag{15}$$

where

$$f_x(t) = \sqrt{2\pi\bar{p}_x w(t_\text{i})\,\frac{\partial t_\text{i}}{\partial t}}\,a(t_\text{i})a(t) \times M^\text{C}\left[\sqrt{\bar{p}_x^2 + \left(\bar{p}_y - \frac{\bar{y}}{\tau}\right)^2}\,\right]\frac{2\text{i}}{\Delta p_\perp \eta}\times \times \exp\left(-\text{i}\bar{S} - \text{i}I_\text{p}\tau + \frac{\text{i}\bar{y}^2}{2\eta}\right) + \text{c.c.}\,, \tag{16}$$

$$f_y(t) = f_x(t)\,\frac{\bar{p}_y - \bar{y}/\eta}{\bar{p}_x} + \text{c.c.} \tag{17}$$

Here, the following notation is used:

$$\eta = \tau - \text{i}\,\frac{2}{\Delta p_\perp^2}\,, \tag{18}$$

$$\bar{S} = \int_{t_\text{i}}^{t} \frac{\bar{p}_x^2(t') + \bar{p}_y^2(t')}{2}\,\text{d}t', \tag{19}$$

$$\bar{p}_{x,y}(t) = \frac{1}{c}\,A_{x,y}(t) - \frac{1}{c}\,A_{x,y}(t_\text{i})\,, \tag{20}$$

$$\bar{y} = \int_{t_\text{i}}^{t} \bar{p}_y(t')\,\text{d}t'. \tag{21}$$

In formulas (16) and (17), $w(t)$ and $a(t)$ are the ionization rate and the amplitude of the atomic ground state at time t, respectively. The latter is written out as

$$a(t) = \left[\exp\left(-\int_{-\infty}^{t} w(t')\,\text{d}t'\right)\right]^{1/2}. \tag{22}$$

The instantaneous ionization rate is found as the ionization rate (in a static field) for the field value taken at some earlier time:

$$w(t_\text{i}) = w\big(|E(t_\text{i} - \delta)|\big)\,. \tag{23}$$

The delay time δ is introduced to take into account approximately the attraction of the free electron to the ionic core after ionization. The value of δ was chosen in Refs [56, 78] so as to achieve the best agreement between the theoretical and numerical results for the generation of UV radiation. The best agreement was achieved with $\delta = 1$ atomic unit of time (≈ 24.2 as); this value is used in all the following calculations. In Ref. [56], the ionization rate $w(E)$ in a static field was calculated using the expression given in Landau's course [79]; in Ref. [78], the tabulated values of the ionization rate were utilized, which were obtained via numerical integration of the Schrödinger equation [45]. Notice that the experimental determination of the 'delay' time of tunnel ionization has recently attracted great attention (see, e.g., Refs [80, 81] and references cited therein).

In expressions (16)–(18), $\Delta p_\perp$ is the uncertainty in the electron's transverse momentum after ionization. The approximate determination of this quantity was made by Perelomov, Popov, and Terent'ev in paper [82] (see also papers [83, 84] and review [85]):

$$\Delta p_\perp^2 = \frac{|E(t_\text{i})|}{\sqrt{2I_\text{p}}}\,. \tag{24}$$

Finally, in expressions (16), (17) one has

$$M^\text{C}(p) = \frac{\mathbf{p}}{p^2}\left\langle \varphi_0(r)\middle|\frac{\mathbf{r}}{r^3}\middle|\psi_\mathbf{p}^\text{C}(\mathbf{r})\right\rangle, \tag{25}$$

where $\psi_\mathbf{p}^\text{C}(\mathbf{r})$ is the Coulomb wave function for a free state with momentum $\mathbf{p}$ before scattering by a Coulomb center (see monograph [79]):

$$\psi_\mathbf{p}^\text{C}(\mathbf{r}) = \exp\left(\frac{\pi}{2p}\right)\Gamma\left(1 - \frac{\text{i}}{p}\right)\exp\left(\text{i}pz'\right) \times F\left(\frac{\text{i}}{p}, 1, \text{i}p(\rho' - z')\right), \tag{26}$$

where $z' = \mathbf{pr}/p$, and $\rho' = \sqrt{r^2 - z'^2}$ are the coordinates of the point $\mathbf{r}$ in a cylindrical coordinate system whose axis is directed along the vector $\mathbf{p}$, F is the confluent hypergeometric function, and Γ is the gamma function.

The ground state (1s) of a hydrogen atom was taken in Ref. [78] as the initial state $\varphi_0(r)$; then, the values of $M^\text{C}(p)$ were found numerically, tabulated, and used for further calculations.

Thus, to calculate the microscopic response at the instant of time t, one should:

(i) find all the ionization instants t_i^m leading to the return at the instant of time t; here, the superscript m labels different ionization instants and corresponding trajectories that lead to a return at the instant of time t (note that the electron energy at a given return time is generally different for different paths). For a monochromatic driving field, the ionization and return instants of time are related to each other according to formulas (2) and (3); for a nonmonochromatic field, one should find them numerically;

(ii) calculate, for the trajectory labelled by m, the values of $\bar{S}^m$ [using formula (19)], $\bar{p}_x^m$, $\bar{p}_y^m$ [using formula (20)], $\bar{y}^m$ [using formula (21)], and $\partial t_\text{i}/\partial t$;

(iii) calculate $f_x^m(t)$ and $f_y^m(t)$ from formulas (16) and (17);

(iv) add up the contributions of different trajectories [see formula (15)].

Let us discuss some of the properties of a single-atom response described by formulas (16) and (17).

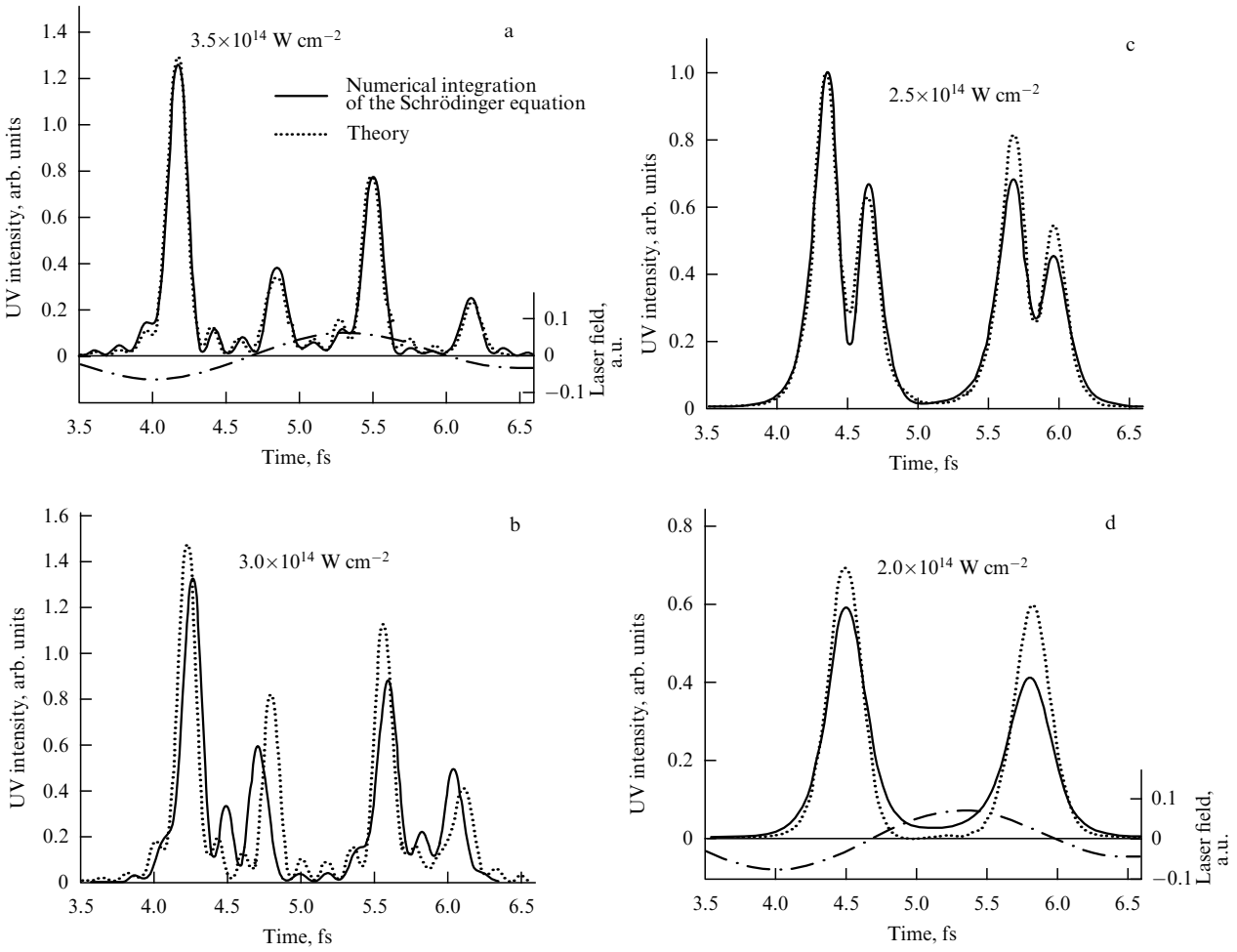

Figure 6. Time profile of the intensity of harmonics in the spectral range from 50 eV (approximately $32\,\hbar\omega_0$) to 75 eV (approximately $48\,\hbar\omega_0$) calculated theoretically (dotted line) and via the numerical solution of the Schrödinger equation for a model argon atom (solid line). Laser field [shown by the dashed-dotted line in figures (a) and (d)] with $\lambda = 0.8$ μm is linearly polarized; peak intensities are marked in the figures; high-frequency cutoff of the plateau is near the harmonics of the order of 53 (≈ 82 eV) (a), 47 (≈ 73 eV) (b), 41 (≈ 63 eV) (c), and 35 (≈ 54 eV) (d). The harmonic intensities in figures (a)–(d) are normalized to the intensity of the first peak in figure (c). (Taken from Ref. [78].)

The factor $a(t_i)a(t)$ in formulas (16) and (17) indicates that the generation occurs only if the ground state is populated at the ionization instant t_i *and also* at the return time t. In Ref. [45], the validity of this conclusion was confirmed by numerical calculations. Notice that the HHG theories [52, 65] do not explicitly contain such a requirement. The reason for this is that these studies assumed adiabatic changes to the ground-state population; hence, the population at the ionization and return instants of time is the same. Obviously, this approximation is not valid if atomic ionization lasts for only several optical cycles.

In Figs 6 and 7, theoretical predictions are compared with the results of numerical integration of the Schrödinger equation (for a model potential of argon [86]). In every half-cycle of the laser field, two attosecond pulses are generated if the selected spectral interval belongs to the plateau region (as noted in the discussion of Fig. 5). These two pulses are generated by short and long electron trajectories [87, 88]. If the selected spectral interval falls entirely within the plateau region, these APs are fully separated (see Fig. 6a); they begin to overlap and interfere if a part of the spectral interval lies in the high-frequency cutoff region (see Figs 6b, c and 7b, c). Finally, these contributions cannot be separated if the entire spectral interval falls within the cutoff region (see Fig. 6d). The duration and timing of APs are in agreement with the numerical calculations. Furthermore, it can be seen in Fig. 6 that the theory discussed here correctly reproduces the ratio between the contributions from different electron trajectories. This is an important difference from Lewenstein's theory [52], which tends to underestimate the role of the short path (as was first noticed by Gaarde and Schafer [89]). This underestimation is apparently due to the neglect of the effect of a Coulomb attraction on the motion of a free electron. It should be recalled that the instantaneous value of the laser field at the instants of time t_i corresponding to a short path is relatively small. If one assumes that it is precisely this field value that determines the ionization rate, then it turns out that the percentage of electrons moving along short paths is also small. In fact, these electrons move a bit more slowly immediately after tunneling due to the Coulomb attraction, i.e., the short paths are 'populated' with electrons that tunnel a little *earlier* than would follow from the classical calculation ignoring the Coulomb attraction by the parent ion. In the present theory, this effect is described by introducing the time delay δ in formula (23). The correct ratio of the contributions from different trajectories provided by this theory is very important when a comparison is made with the experimental data. It is worth mentioning that a similar way to take into

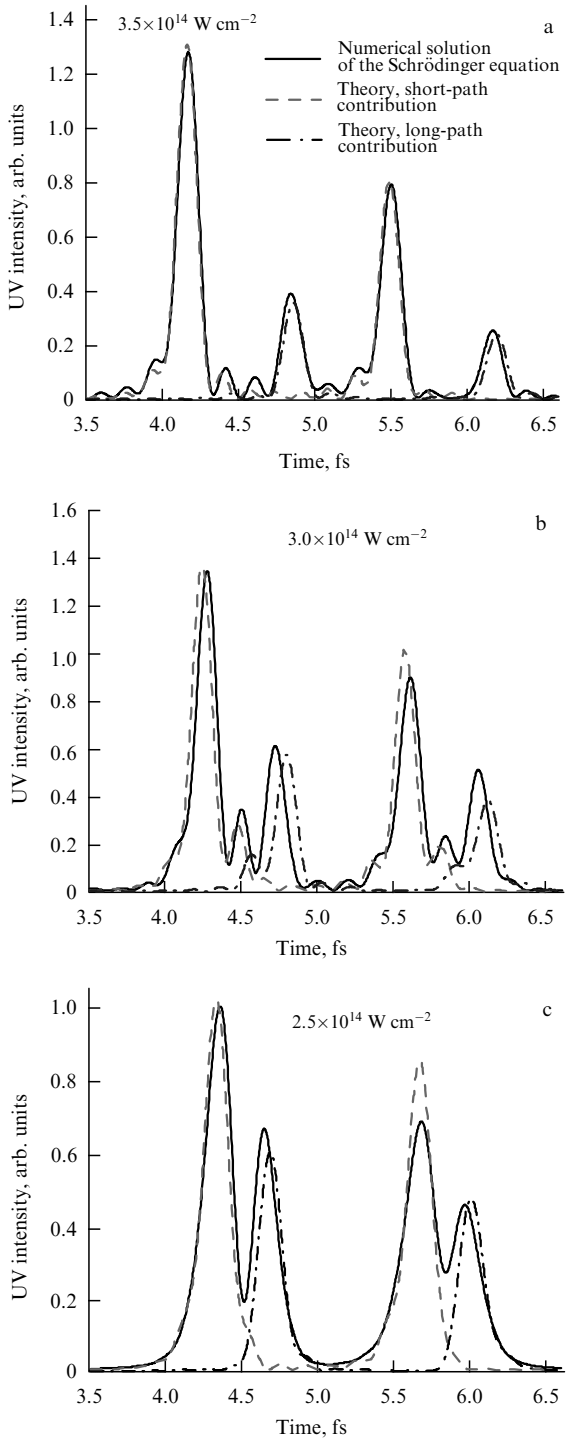

Figure 7. Same as in Fig. 6, but the theoretical curves represent separately the contributions from two quantum trajectories corresponding to the electron's excursion times shorter than an optical cycle: the dashed and dashed–dotted lines show the short- and long-path contributions, respectively. (Taken from Ref. [78].)

account the Coulomb attraction in the process of electron detachment [90] allowed achieving good agreement with experiment [91] when the semiclassical model was constructed to describe the production of directional photocurrents giving rise to THz wave generation in the optical breakdown of gases.

Thus, we can conclude that there is good quantitative agreement between theory and numerical calculations for HHG in a laser field with a wavelength of about 800 nm (Ti: sapphire laser) and intensity on the order of 10^{14} W cm^{-2} ($\gamma \approx 1$). This agreement demonstrates the applicability of the assumptions made in this theory at those values of the laser field parameters, which are quite typical for HHG.

The above theory [78] was successfully applied to describe HHG from atoms in an elliptically polarized laser field, showing very good agreement with the numerical results [48, 50]. In particular, this theory allowed explaining the origin of ellipticity of harmonic polarization [50] and describing the influence of the ellipticity of the laser field on the efficiency of HHG and the state of polarization of high harmonics for atoms with different types of valence orbitals [48].

At the end of this section, we will briefly describe the current areas of further development of the aforementioned and other theoretical approaches.

In recent years, increasing attention in the context of high-order harmonic generation has been paid to molecules as more complex systems than atoms, which provide additional means to control the HHG process [92–99], inaccessible when utilizing atomic gases as a working medium. In the molecular case, the magnitude of the high-order harmonic signal [92, 95] and its spectral [93, 94, 100, 101], temporal [98], and polarization [99] properties can highly depend on the relative positions of the nuclei in a molecule and the orientation of the molecular axes with respect to the laser electric field (these dependences often occur due to multicenter interference effects [93, 94]; there may also be a significant contribution to HHG from the ionization of multiple molecular orbitals [102]). The HHG spectra and the temporal dynamics of the AP generation in molecules may also exhibit effects associated with the motion of nuclei during laser pulse propagation [96, 97, 103–105]. It has been demonstrated that many of the effects mentioned above may be employed to probe the structure and ultrafast internal dynamics of molecules with subfemtosecond temporal and angström spatial resolutions (see reviews [106, 107]). Due to the complexity of the molecule as an object of the theoretical study of HHG and other strong-field processes, it is very important to develop analytical methods for the approximate description of these phenomena. In recent years, such methods have been developed extensively. For example, the first attempts were made in Refs [104, 108–110] to generalize Lewenstein's theory and other analytical theories in order to provide a description of high-order harmonic generation in molecular gases. However, a detailed discussion of these issues is beyond the scope of this review.

The above results were usually obtained in the one-electron approximation. State-of-the-art computer capabilities also allow the numerical solution of two-electron problems [111–116]; however, direct numerical calculations cannot be implemented in the case of a larger number of electrons. One of the approaches to the analytical description of multielectron effects is based on the fact that these effects manifest themselves in the HHG spectra basically only through the energy dependence of the cross section of electron–ion recombination (i.e., of the process being the final stage of the three-step mechanism of HHG) [60, 117–120]. The recombination cross section can be calculated separately for a specific atom (notably, on the basis of the principle of detailed balance, it can be found from the experimentally determined photoionization cross section; the restrictions on this approach were discussed in Refs [121–124]). Among the consequences of this approach related to

multielectron effects was the prediction of giant dipole resonance near 100 eV in the HHG spectrum of xenon; this prediction was confirmed experimentally in Ref. [125]. The multielectron effects can be particularly significant when the harmonic frequency is close to resonance with one of the natural frequencies of the nonlinear medium, as was pointed out in Ref. [126]. Various mechanisms of resonance-enhanced HHG have been theoretically studied in Refs [127–129]. A significant (up to two orders of magnitude) increase in the efficiency of the generation of the harmonic at a frequency close to the transition frequency between the ground and autoionization states of generating ions was observed experimentally in studies of HHG in a plasma plume (see review [130] and references cited therein). Theoretical models of this process were proposed in Refs [119, 131–133]. Paper [132], in particular, reported on the so-called 'four-step' model of resonance-enhanced HHG; the phase locking of harmonics near resonance was studied, resulting in the conclusion that resonant harmonics are produced as a train of APs. Further development and validation of this model can be found in Refs [134, 135].

2.4 Macroscopic response. Phase matching in high-order harmonic generation

In the problem of harmonic generation, as in a number of other problems of nonlinear optics [136, 137], it is not only microscopic (relating to the nonlinear response of an individual atom or molecule) factors that are of great value; macroscopic factors also play an important role. One of the main issues of this kind concerns with phase matching. In particular, due to the difference in phase matching of different harmonics, the experimentally observed spectrum can differ very significantly from the spectrum of a single-atom response. For efficient frequency conversion in a nonlinear medium, it is important that the generated frequency components propagate through medium with the same phase velocity as the driving wave, since in this case the coherent summation of the signals from the elementary emitters leads to the accumulation of the resulting signal as the interacting waves propagate in the macroscopic volume of the medium.

Thus, the formulation of the problem of phase matching in HHG is similar to that for other nonlinear optical processes. In the absence of phase matching, the signal can only enhance as it propagates through a nonlinear medium, unless the phase shift between the driving and generated waves exceeds π radians. The coherence length $L_{\rm coh}$ in the given region of medium is inversely proportional to the phase mismatch between the wave vectors of the interacting waves, which in the case of the generation of a high harmonic of order q is written as $L_{\rm coh} = \pi/\Delta k_q$, where Δk_q is the wave-vector mismatch. One of the main reasons for the phase mismatch in the nonlinear-optical frequency conversion of laser light is the dispersion of the nonlinear medium utilized for this transformation. It is well known [136] that phase matching for low-order harmonic generation or other nonlinear optical processes of low order can be implemented using birefringent media. In the problem of interest to us, i.e., high-order harmonic generation in gases, this approach is not feasible due to the isotropy of the gas medium. Moreover, there are a number of additional factors causing the phase mismatch in HHG.

First, as mentioned in the previous section, the dipole moment at the harmonic frequency undergoes a phase shift Φ (usually called quantum or atomic phase) with respect to the driving field [88, 138–141]; this shift depends on the laser radiation intensity. For each quantum-mechanical trajectory contributing to the generation of the given harmonic, this dependence is approximately linear [see formula (12)]. The change in intensity of the driving field along the propagation axis thus leads to an addition to the wave-vector mismatch: $\partial\Phi/\partial z = -\alpha_{\rm s}\partial I/\partial z$. Due to the significant difference among the values of $\alpha_{\rm s}$ on different trajectories, the phase mismatch can be small for the contribution from only one of these trajectories (if the value of $\partial I/\partial z$ is not small and, hence, the term discussed here is significant). It should be noted that the intensity of the driving field also depends on time t and on the distance r from the beam axis; hence, the dependence of Φ on the intensity leads to the spectral shift of the harmonic, $\partial\Phi/\partial t = -\alpha_{\rm s}\partial I/\partial t$, and to an additional divergence: $\partial\Phi/\partial r = -\alpha_{\rm s}\partial I/\partial r$. This allows the selection of the contribution from the particular electron trajectory in the experimental HHG spectrum [142, 143].

Second, the HHG mechanism implies ionization of the particles in the medium. As a result of ionization, the plasma, in addition to the neutral component, emerges in the medium, making its own contribution to the wave dispersion in the medium. Moreover, since the dispersion properties of a neutral gas and plasma differ greatly, the change in their relative concentrations during the laser pulse action causes the instability of the refractive index of the medium. The dispersions of a neutral gas and plasma have different signs; for the case of HHG driven by near-IR sources, they cancel each other out at a very low degree of ionization (a few percent), which in practice limits the laser intensity usable for HHG.

Third, the analysis of phase matching for HHG should take into account the phase shift (Gouy phase, or geometric phase) acquired by the laser beam as it passes through the focus. The dependence of this phase on the coordinate along the propagation axis gives rise to the so-called 'geometric' term δk_0 in the wave vector of the driving field. For a Gaussian beam, one obtains

$$\delta k_0(z) = -\frac{\lambda_0}{\pi a_{\rm e}^2(z)}\,, \tag{27}$$

where $a_{\rm e}$ is the beam radius at the field level of e^{-1}.

Fourth, the harmonic beam divergence may be large enough (see below), which makes it necessary to take into consideration the *off-axis* phase matching.

Taking into account all these factors, we can write down the phase mismatch (a more rigorous analysis will be given below) for the harmonic component propagating at an angle θ to the beam axis in the form

$$\Delta k_q(z,t) = q(k_0 + \delta k_0) - k_q\cos\theta + \alpha_{\rm s}\frac{\partial}{\partial z}I\,, \tag{28}$$

where $k_0 = n_0\omega_0/c$ and $k_q = n_q q\omega_0/c$ are the lengths of the wave vectors of a plane wave at the frequency of the driving field and the harmonic frequency, respectively; n_0 and n_q are the refractive indices at these frequencies.

Notice that the phase matching condition $\Delta k_q \approx 0$ represents the condition of conservation of the axial momentum component in the transformation of q laser photons into the harmonic photon.

From equation (28) it follows how sensitive the HHG process is to the generation conditions: marked phase mismatch occurs even in cases of a rather small difference

$n_0 - n_q$ in the refractive indices or small geometric term δk_0, because they are multiplied by a *large* harmonic order q.

In HHG using a focused beam, conditions may arise under which the atomic and geometric phases cancel each other out in a certain area on the propagation path. Such conditions can be met at some places behind the focus, where the intensity of the laser beam decreases with distance [141]. Nevertheless, the tapping of tightly focused laser beams has the substantial disadvantage lying in the fact that the interaction length along which high harmonics are generated is restricted to a very narrow region around the focus where the laser radiation intensity is sufficient for HHG.

To carry out a rigorous quantitative analysis of phase matching, we proceed from the wave equation

$$(\nabla^2 + k_q^2)E_q = -\frac{\mathrm{i}4\pi q\omega_0 \tilde{j}_q}{c^2}\,,$$

where $\tilde{j}_q$ is the density of the laser-induced nonlinear current at the harmonic frequency.

The expression for the current density $\tilde{j}_q$, which contains the phase factors (present in the driving field) raised to the qth power, can be written as the product:

$$\tilde{j}_q(z,\rho) = j_q\big(I(z,\rho), N(z,\rho)\big)\exp\left[\mathrm{i}q\big(k_0 z - \varphi(z) + \phi(z,\rho)\big)\right], \tag{29}$$

where

$$\phi(z,\rho) = k_0\,\frac{\rho^2}{2R(z)}\,; \tag{30}$$

$N(z,\rho)$ is the gas density; $R(z)$ and $I(z,\rho)$ are the radius of the wave front and the intensity of the driving beam, respectively; $\varphi(z)$ is the phase shift, which depends on the beam structure, and the amplitude j_q is, in general, complex and dependent only on the radiation intensity I and the properties of the medium. The amplitude j_q of the current is related to the amplitude of the atomic response (quantum-mechanical average of the force acting on the electron) as

$$j_q = \frac{\mathrm{i}f_q N(z,\rho)}{\omega_q}\,. \tag{31}$$

In some approximations (see papers [17, 78]), the radiation power emitted at the harmonic frequency can be written down as

$$P_q = \int p_q(\theta)\theta\,\mathrm{d}\theta\,, \tag{32}$$

where

$$p_q(\theta) = \frac{1}{c^3}\left|\int_{z_1}^{z_2}\exp\left[\mathrm{i}z\left(qk_0 - k_q + k_q\,\frac{\theta^2}{2}\right) - \mathrm{i}q\varphi(z)\right]g_q(\theta,z)\,\mathrm{d}z\right|^2. \tag{33}$$

Here, z_1 and z_2 are the coordinates of the target ends, and

$$g_q(\theta,z) = 2\pi\int f_q\big(I(z,\rho)\big)N(z,\rho)\exp\big(\mathrm{i}q\phi(z,\rho)\big)J_0(k_q\rho\theta)\rho\,\mathrm{d}\rho\,, \tag{34}$$

where J_0 is the zero-order Bessel function. The function $g_q(\theta,z)$ can be interpreted as the angular spectrum of the emission at the qth harmonic frequency, generated by a thin layer in the beam cross section at a point with coordinate z.

Expressions (33) and (34) are applicable in the quasistatic case, i.e., when the parameters of the laser and harmonic fields vary slowly or, in other words, when the processes causing emission proceed quasiperiodically over many cycles of the laser field. If this is not the case, then, obviously, a continuous spectrum rather than a set of harmonics is emitted. In that event, similar calculations lead, instead of to expressions (33) and (34), to

$$p_\omega(\theta) = \frac{1}{c^3}\left|\int_{z_1}^{z_2}\exp\left\{\mathrm{i}z\,\frac{\omega}{c}\left[\tilde{n}_0 - \tilde{n}\left(1 - \frac{\theta^2}{2}\right)\right]\right\}g_\omega(\theta,z)\,\mathrm{d}z\right|^2, \tag{35}$$

$$g_\omega(\theta,z) = 2\pi\int f_\omega N(z,\rho)\,J_0(k\rho\theta)\rho\,\mathrm{d}\rho\,. \tag{36}$$

Here, $\tilde{n}_0$ and $\tilde{n}$ are real parts of the refractive index at the frequency of the laser radiation and at the frequency ω, respectively, and $k = \tilde{n}\omega/c$ is the wave vector at the frequency ω. It should be noted that in formulas (35) and (36) we made use of the amplitude f_ω of the microscopic response dependent on the laser field $E_0(z,\rho,t)$ [which is why the phase of the laser field does not enter explicitly into Eqns (35) and (36), in contrast to Eqns (33) and (34); the phase of the laser field determines the phase of the microscopic response amplitude f_ω]. Expressions (35) and (36) may be utilized when the microscopic response is not periodic with the period equal to the laser cycle. The microscopic response amplitudes in this case are calculated numerically:

$$f_{x,y}(\omega) = \frac{1}{2\pi}\int f_{x,y}(t)\exp(\mathrm{i}\omega t)\,\mathrm{d}t\,. \tag{37}$$

The atomic dipole moment as a function of time can be calculated according to the formulas (10) or (16) and (17).

As a rule, the efficiency of UV emission via HHG is limited mostly by the phase-matching conditions. In some cases, however, the absorption of the radiation in the nonlinear medium also plays an important role. In these conditions, the imaginary part of the refractive index n_{abs} at the frequency of the generated radiation should be also taken into account. Then, instead of expression (36), we have

$$g_\omega(\theta,z) = 2\pi\exp\left[-\frac{\omega\tilde{n}_{\mathrm{abs}}(z_2 - z)}{c}\right]\int f_\omega N(z,\rho)J_0(k\rho\theta)\rho\,\mathrm{d}\rho\,. \tag{38}$$

Now we will discuss the question under what parameters the off-axis phase matching can play a significant role in HHG. Obviously, the off-axis phase matching is necessary to take into account if [see formula (33)] the θ-angle-dependent phase shift accumulated across a target of thickness $\tilde{z} = z_2 - z_1$ is greater than $\pi/2$:

$$\tilde{z}k_q\,\frac{\theta^2}{2} > \frac{\pi}{2}\,.$$

Maximum value of the angle θ corresponds to the harmonic divergence. Roughly taking the latter equal to the laser beam divergence, one finds [144] that

$$\tilde{z} > \frac{b}{q}\,, \tag{39}$$

where b is the confocal parameter of the laser beam.

It can be seen from condition (39) that the higher the harmonic order, the smaller the thickness of the target for which the off-axis phase matching can still be ignored. Typically, condition (39) is fulfilled in experiments on HHG; hence, an analysis of the off-axis phase matching is valuable for their interpretation.

We carried out a detailed theoretical analysis of the phase matching in HHG in Refs [88, 142, 145–147]. It was shown that the range of angles for which the harmonics are generated efficiently narrows with increasing generating layer thickness; hence, the harmonic power increases more slowly than quadratically with layer thickness. In other words, only those angular components of the harmonic are generated synchronously, which fall within a limited interval narrowing with increasing thickness of the layer.

Studies of HHG were carried out in Refs [142, 148–150] for the case of a driving field propagating in a gas-filled hollow waveguide (capillary). In this case, the geometrical term (27) entering the dispersion relation is replaced by the so-called waveguide term which has the same sign:

$$\delta k_0(z) = -\frac{u^2\lambda_0}{4\pi a^2}\,, \tag{40}$$

where a is the radius of the waveguide, and u is the coefficient determined by the regime of the driving field in the waveguide. This regime is of great interest in the context of HHG because, in this case, the laser beam is capable of propagating over a relatively large distance without divergence. Moreover, taking advantage of a capillary allows the solution to the technical problem of creating a target containing gas under fairly high pressures (ranging from a few to some tens of atmospheres). In this case, there can be a considerable number of harmonic emitters even at a low degree of ionization, when, as mentioned above, the dispersion of plasma and geometric dispersion can still be cancelled out by the dispersion of neutral atoms. By implementing experimentally this scheme, the harmonics have been produced with the highest orders (up to about the 5000th harmonic [151]) to date.

At radiation intensities sufficient for HHG, the driving laser pulse can propagate in the self-channeling regime. Similar to the capillary case, an increase in the interaction length leads to a relatively high efficiency of harmonic generation [145, 152].

When the phase matching of the interacting waves is out of reach, the quasiphase matching technique can be applied for solving the problem, at least partially. This approach, which is widely used in the optical frequency range, implies a periodic (with a period determined by the coherence length) spatial modulation of the nonlinear properties of the medium. This modulation is carried out so that the generation occurs efficiently only in those areas of the medium whose contributions to the signal interfere *constructively*. Different ways of extending this approach to the problem of high-order harmonic generation have been demonstrated, among which are the use of waveguides with a periodically modulated diameter [153, 154], noncollinear HHG (analyzed by our team in papers [155, 156] and recently implemented experimentally [157, 158]), modulation of laser light via excitation of higher regimes of the waveguide [159], the employment of multijet gas targets [160, 161], and others. A more detailed discussion of the macroscopic aspects of the high-order harmonic generation process can be found in reviews [162, 163].

The synchrony in the production of UV emission via HHG can, in general, vary during the laser pulse transmission because of ionization of the medium [149, 164–166]. The time interval within which the harmonic generation occurs synchronously and, hence, efficiently, can be quite short. This, on the one hand, restricts the possibility of enhancing the efficiency of HHG thanks to canceling out the plasma dispersion by the dispersion of neutral atoms. On the other hand, if the above-mentioned time interval is comparable to half of the optical cycle, the efficient generation of a single AP occurs.

When analyzing the synchrony of the harmonic generation with the aid of formula (28), we assumed the refractive index of the medium to vary only slightly during the laser radiation period, whereas the harmonic phase shift Φ was assumed to depend only on the intensity of the driving pulse (and did not depend on the duration and shape of the pulse). These assumptions may become invalid in the case of harmonic generation driven by a few optical cycle laser pulse. The tools for the analysis of phase matching in this case were developed in Ref. [167]. A significant change in the refractive index during the optical cycle causes a change to the intracycle time dependence of the field, which, in turn, strongly influences the phases of the harmonics. In this case, the so-called self-phase-matching regime investigated theoretically by Tempea et al. [168] can be realized.

2.5 High-order harmonic generation and attosecond pulse production in a few-micrometers long wavelength laser field

Until recently, almost all experiments on HHG were carried out making use of the Ti:sapphire laser. In recent years, however, there has been growing activity in the development and applications of sources delivering intense femtosecond pulses with a central wavelength of one to a few micrometers [169–174]. In Sections 2.5.1–2.5.6, we briefly discuss the prospects for AP production using these sources and the first results obtained in this direction.

2.5.1 Width of the plateau. The maximum energy of a photon produced via HHG is determined by the ponderomotive energy of an electron in the driving laser field, which is proportional to the product of laser radiation intensity I and the square of its wavelength λ: $U = E_0^2/(4\omega_0^2) \propto I\lambda^2$. The possibility of extending the plateau towards higher frequencies by increasing the intensity of the driving laser is limited by the rapid growth of the tunneling ionization rate with intensity. Ionization of the gas results in (a) a reduction in the number of atoms involved in the process of harmonic generation, (b) an increase in the phase mismatch associated with the presence of free electrons, and (c) defocusing of the laser beam.

An alternative method of producing higher-order harmonics involves the use of laser light with longer λ, which was first experimentally demonstrated in Refs [175, 176]. Exploiting a laser source with $\lambda = 1.6$ μm, the generation of harmonics in the 'water window' from neutral gases was demonstrated for the first time [177] (in experiments on HHG driven by a Ti:sapphire laser, the generation of harmonics within the 'water window' was achieved only with ions as a nonlinear medium), whereas the tapping of a laser source with $\lambda = 3.9$ μm has allowed for the first time the production of high-brightness harmonic emission with photon energies up to 1.6 keV [151].

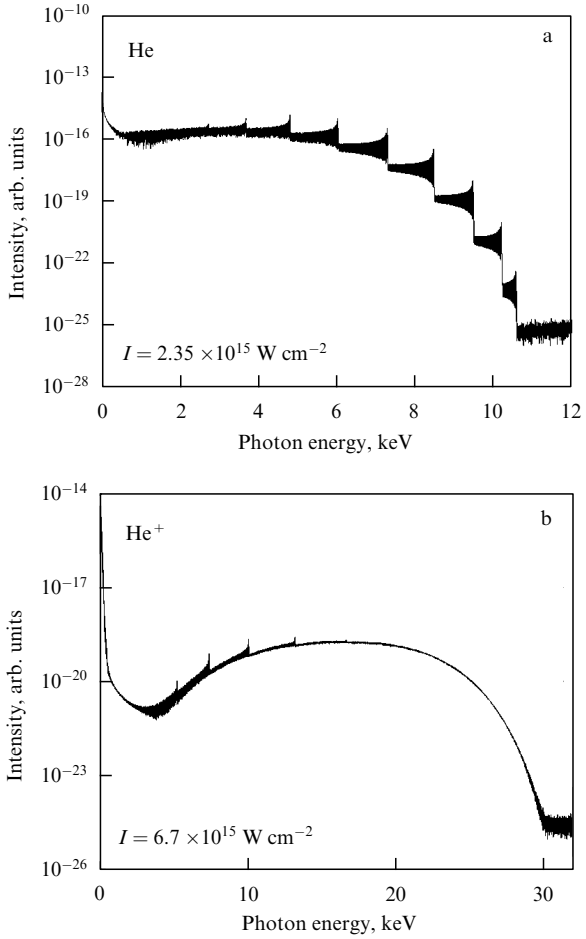

Figure 8. Harmonic spectra calculated analytically for (a) an He atom, and (b) an He^+ ion, driven by a linearly polarized Gaussian laser pulse with the duration of 6 optical cycles, central wavelength of 3.9 μm, and peak intensities of 2.35×10^{15} and 6.7×10^{15} W cm^{-2}, respectively.

At sufficiently long λ, the effect of the magnetic field of the laser pulse becomes the other important factor restricting the width of the spectrum of the generated harmonics [178]. This effect manifests itself, in terms of the classical theory, in the distortion ('magnetic drift') of the electron trajectories and, as a consequence, in a reduced probability of electron collisions with the parent ions and emission of high-energy photons [179, 180]. The role of this factor raises with increasing ionization potential I_p of the particles of a nonlinear gaseous medium. In the conditions of magnetic-drift limited high-order harmonic generation, the reduction in the number of electron trajectories contributing to HHG leads to the formation of an arc-like harmonic spectrum instead of a plateau [178, 181], which, in fact, means the narrowing of the effective width of the spectrum of the generated harmonics. This is illustrated in Fig. 8, which displays the spectra of high-order harmonics generated in neutral (see Fig. 8a) and ionized (see Fig. 8b) helium at $\lambda = 3.9$ μm and at high peak intensities of the laser pulse (the pulse was assumed to be Gaussian, with FWHM equal to six optical cycles). The calculations were carried out using the modified strong-field approximation, which, in contrast to Lewenstein's theory [52], takes into account the atomic bound-state depletion and the magnetic-drift effect [178]. According to these calculations, for neutral helium ($I_p = 24.6$ eV) driven at $\lambda = 3.9$ μm, the dominating factor restricting the magnitude and spectral width of the nonlinear response is the depletion of atomic energy levels. As a result of a progressive jump-like depopulation of the atomic bound states, occurring at the electric field maxima on the leading edge of the laser pulse, the harmonic yield declines stepwise with increasing photon energy (see Fig. 8a); the maximum photon energy of the most intense part of the harmonic emission spectrum ranges 5–7 keV. In the case of ionized helium ($I_p = 54.4$ eV), the electric field required to liberate an electron is so high that the oscillation velocity of a free electron driven at $\lambda = 3.9$ μm is comparable with the speed of light. This leads to a strong magnetic drift of the electron and, therefore, to the formation of an arc-shaped HHG spectrum (see Fig. 8b); in this case, a relatively efficient generation of harmonic photons with energies of about 15–20 keV is expected [182]. The calculations for even higher λ indicate that, for example, at $\lambda = 10.6$ μm (CO_2 laser) HHG is greatly affected by the magnetic field even in the case of neutral atoms [178].

2.5.2 Magnitude of the atomic response. The possibility of generating higher-energy harmonic photons by exploiting longer-wavelength laser sources is severely limited by a rapid decrease in the magnitude of a high-frequency atomic response and, consequently, in the intensity of the harmonics with increasing laser wavelength. This, to a large extent, is due to the spreading of the electron wave packet on the stage of free motion: obviously, this spreading is greater for a longer optical cycle. Both theoretical [45, 183–187] and experimental [188, 189] studies revealed that the intensity of the harmonic emission in a given spectral range decreases with increasing λ as λ^{-x}. The numerical value of $x = 5-6$ for the exponent of the power-law scaling of the harmonic yield was obtained in the theoretical calculations of atomic nonlinear response for different atoms [45, 184, 185, 187]. In experiment [189], the role of factors related to the gas density (and, therefore, the phase mismatch) was minimized. Nevertheless, an even faster decrease in the intensity of harmonics in the spectral window of 16 to 32 eV ($x = 6.3-6.5$) was observed. However, as a theoretical analysis predicts [119], the above-mentioned unfavorable tendency can be greatly mitigated in multielectron atoms thanks to the anomalously large cross sections of free–bound electronic transitions in certain intervals of electron energies. For instance, calculations give evidence that the efficiency of frequency conversion of laser radiation into the vacuum ultraviolet range in xenon can be several orders of magnitude higher than in other noble gases due to the presence of giant resonance in the cross section of free–bound transitions at electron energies on the order of 100 eV. This finding has been confirmed in a recent experiment [125].

2.5.3 Attosecond chirp. According to the semiclassical model of HHG, the group delay dispersion of high-order harmonics (chirp of attosecond pulses, or attochirp) should decrease with the driving laser wavelength as $1/\lambda$, which was confirmed by experimental measurements [190]. Because of this, when using a longer-wavelength driving field with the same intensity, (i) shorter APs compared to the case of a shorter-wavelength driver can be obtained when the attochirp compensation is not carried out, and (ii) the implementation of attochirp compensation becomes easier.

2.5.4 Phase matching. When exploiting long-wavelength sources, the problem of phase matching appears to be particularly serious, because the generated radiation with a given wavelength is obtained as a harmonic of higher order

than in the case of a Ti:sapphire laser utilized as a driver; accordingly, the phase mismatch (28) is even more sensitive to the generation conditions. However, an important feature of this regime is that, in order to generate radiation with a given wavelength, lower laser intensity is needed. Consequently, the degree of ionization of the atoms in the medium may be significantly reduced. The employment of high-density gas targets allows a partial compensation for the reduction in the magnitude of the microscopic response with increasing λ and with decreasing intensity of the driving field [151, 191].

The use of long-wavelength lasers for driving HHG entails an increased role of nonadiabatic effects in phase matching in the case of a few-cycle laser field. As the calculations revealed [192], under certain conditions it can result in an efficient high-order harmonic generation within a short time window lasting for one or a few half-cycles of the driving field.

2.5.5 Isolated attosecond pulse production via polarization gating. The threshold ellipticity decreases with increasing λ [48]. This facilitates the production of isolated APs via polarization gating [193].

2.5.6 Spectroscopic applications of HHG. One of the spectroscopic applications of HHG relies on the observation of the multicenter interference minima in the spectra of harmonics generated in molecular gases [93, 94, 194, 195]. The positions of these minima depend on the internuclear distances in molecules, allowing the extraction of information about the molecular structure from the measured HHG spectra. Since the maximum experimentally attainable width of the HHG spectrum is restricted by the saturation intensity at which the molecular ionization occurs, for molecules with a relatively low ionization potential such measurements with a Ti:sapphire laser are hampered by the narrowness of the plateau. Making use of longer-wavelength driving lasers allows the generation of a wider plateau suitable for extracting information about the structure of these molecules (see recent experiments [196]).

Important for spectroscopic applications is also the fact that a smaller energy of the pumping laser photon yields a denser frequency comb in the harmonic spectrum, which actually (i) means a finer frequency tuning of the generated radiation, and (ii) provides higher spectral resolution in measurements utilizing interference patterns in the HHG spectra.

3. Attosecond pulse generation through the interaction of a laser pulse of ultrarelativistic intensity with the surface of high-density plasma

3.1 Introduction

As already mentioned in Section 2, the APs generated in gases have low power, which constraints their application in a physical experiment. It is expected that taking advantage of a reflection of short relativistically intense laser pulses from the surface of condensed-phase targets will allow the generation of APs with significantly higher intensities and lower durations, including isolated (i.e., single) pulses in the near future. The possibility of efficient generation of such APs was convincingly demonstrated in numerical calculations.

In this research area, the 'particle-in-cell' (PIC) numerical method is widely applied. In this method, the plasma is represented as a set of large quasiparticles with a charge-to-mass ratio equal to this ratio for real particles (electrons and ions). The quasiparticles interact with each other, not directly but through electromagnetic fields radiated by them. The fields are determined from the Maxwell equations defined on Euler's coordinate grid. The equations of motion for quasiparticles are written down in the relativistic form. The serial numbers of quasiparticles can be considered as their Lagrangian coordinates. A detailed description of the method can be found in monographs [197, 198]. In the above-mentioned simulations, the target is usually modelled by a layer of dense (supercritical) plasma with the given initial parameters.

Physical experiments have not yet demonstrated the generation of isolated APs on the plasma surface. It was shown in experiments [28, 29] that the high-order harmonics (HHs) generated on the target surface irradiated by laser pulses with a duration of 45 fs are phase-locked and are emitted as an AP train.

In contrast to harmonic generation in gases, HHs from the plasma surface are classical in nature, and qualitative models applied to explain them are relatively simple. However, a quantitative description of the phenomenon faces serious difficulties. It is challenging to find any reliable analytical solutions of a complex set of equations describing this phenomenon, whereas a numerical study is highly demanding. Moreover, the mechanism of the phenomenon is ambiguous and depends on the experimental conditions.

At subrelativistic intensities (intensity referred to as subrelativistic is that satisfying the condition $I < I_{\rm rel}$, where $I_{\rm rel} = [c/(8\pi)](mc\omega/e)^2 \approx 1.37 \times 10^{18}\,(1\ \mu{\rm m}/\lambda)^2$ [W cm^{-2}]), the generation of HHs is apparently governed by the 'coherent wake emission' (CWE) mechanism [199], which, in brief, is as follows. When the surface of a condensed-phase target is exposed to intense light, electron bunches arise in an expanding plasma, which penetrate deep into the plasma [200] and excite plasma oscillations with frequencies that are multiples of the bunch repetition frequency and, hence, the frequency of light. In inhomogeneous plasma, the plasma oscillations are partially transformed into electromagnetic waves leading to the HH emission. The frequencies of HHs are bounded by the plasma frequency ($\Omega_{\rm pl} = \sqrt{4\pi Ne^2/m}$, where N is the plasma concentration) and are relatively low. The CWE proceeds most efficiently at the oblique incidence of p-polarized light on the target.

At relativistic intensities ($I > I_{\rm rel}$), the generation of HHs with frequencies not bounded by the plasma frequency is possible [201, 202], which makes this generation regime more interesting in terms of producing APs (including isolated ones). To explain the HH generation in this regime, the 'oscillating mirror' model was proposed [203]. This model assumes that the electron spatial distribution has a sharp border which oscillates against immobile ions. The surface oscillations cause Doppler frequency shifts which determine the spectrum of the reflected light.

Under certain conditions, the plasma evolution in the relativistic regime turns out to be correlated with the laser field in such a way that ultradense electron nanobunches are formed near the plasma–vacuum interface [204–207], which release the energy accumulated by them in a process analogous to synchrotron radiation. Thanks to the narrowness of these bunches, all the electrons within them are emitted coherently; the emission spectrum in this case is characterized by a slower decrease in intensity with the

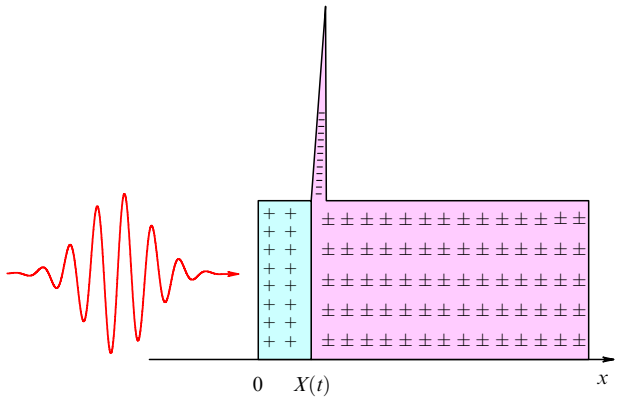

Figure 9. Distribution of electrons and positive charges in the plasma. The positive charge border (plasma–vacuum interface) is located in the plane $x = 0$, the electron component border $X(t)$ moves in the region of $x \geqslant 0$, in accordance with the field strengths. The electrons that were originally in the region between 0 and $X(t)$ are grouped in a thin layer around the coordinate $X(t)$.

harmonic order [204, 208] than in other cases mentioned above. For this reason, the process underlying this regime of HHG is singled out as one more HH generation mechanism called 'coherent synchrotron emission'. The physics of processes leading to the production of APs in this regime with an oblique incidence of light on a plasma surface was discussed in detail in Refs [204, 206]. In particular, the 'relativistic electron spring' model was proposed [206], which describes the accumulation and release of energy in the near-surface plasma layer compressed by the light pressure force.

A detailed discussion and comparison of the above mechanisms of HH generation on a plasma surface and their theoretical description can be found in recent reviews and original papers [25, 26, 209, 210]. The theory presented below describes HHG on the edge of dense plasma in the parameter range typical for the model of a relativistic oscillating mirror.

3.2 Analytical model

Electron motion activated by incident light is influenced by the intensity and frequency of light, the plasma density, and other factors. Analytical models describing the electron motion are usually based on a rather simplified picture of this motion. Typically, the construction of such models implicitly assumes that the laser pulse comprises many field cycles and that the plasma surface oscillations are periodic in time.

We will discuss here an alternative model, assuming that the laser pulse duration is short (two or three optical cycles), plasma motion is not periodic, and the frequency and intensity of light are not too great, so that the electron movement is only restricted by potential fields (not inertia). We assume that the plasma is fully ionized. Before the arrival of the electromagnetic pulse, the sharp edge of the plasma resides at $x = 0$ (see Fig. 9). We also assume that the plasma density is very high, so that the skin layer thickness can be considered arbitrarily small, the critical plasma frequency is much higher than the frequency of light, and the displacement of electrons induced by the light pressure is many times smaller than the laser wavelength. Under these conditions, the position of the border of the electron component adiabatically tracks the change in light pressure, and its coordinate $X(t)$ can be found from the equation

$$P_{\text{light}}(t, X) = P_{N_e}(X)\,, \tag{41}$$

where $P_{\text{light}}(t, X) = [(1 + R)/(4\pi)]E^2_{\text{inc}}(t - X/c)$ is the pressure of light reflected from the border of the electron component, $E_{\text{inc}}(t)$ is the electric field strength of the incident wave in the plane $x = 0$, R is the reflectivity (hereinafter, it is assumed that $R \approx 1$), $P_{N_e}(X) = 2\pi(N_e e X)^2$ is the surface density of potential forces that keep the electron component from further displacement, and N_e is the initial electron concentration.

When postulating condition (41), we disregard the term on the right-hand side which takes into account the inertia of the electrons, i.e., the term $\mathrm{d}P/\mathrm{d}t$, where P is the electron momentum surface density. This is valid at relatively high densities N_e utilized in the calculations.

Equation (41) can be easily solved numerically. Let $X(t)$ be the solution of this equation, and $E_{\text{ref}}(t)$ the electric field strength of the reflected wave in the plane $x = 0$. Then, one finds

$$E_{\text{ref}}\left(t + \frac{X(t)}{c}\right) = E_{\text{inc}}\left(t - \frac{X(t)}{c}\right). \tag{42}$$

Using relationship (42), one can simulate numerically the dependence $E_{\text{ref}}(t)$.

3.3 Numerical results

3.3.1 Normal incidence. Sharp plasma-vacuum boundary. Figure 10 plots the dependence $E_{\text{ref}}(t)$ obtained with the aid of the model described in Section 3.2 for the incident pulse given by

$$E_{\text{inc}}(t) = a\,\frac{mc\omega}{e}\exp\left[-(3.4\pi\omega t)^2\right]\sin(\omega t)\,, \tag{43}$$

with $\lambda = 0.8$ μm, $a = 15$, and $N_e = 10^{23}$ cm^{-3}.

It is seen that the overoscillations of the reflected field become saw-toothed with increasing incident field amplitude. It appears that the time intervals at which the electric field modulus $|E_{\text{ref}}|$ rises are lengthened, as well as the intervals at which it falls are shortened, exhibiting increasingly sharp

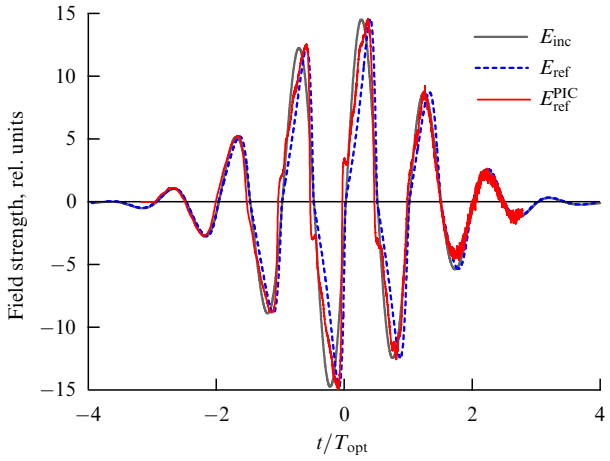

Figure 10. (Color online.) Incident (gray line) and reflected fields calculated using relationship (42) (dashed line) and by the PIC method (solid red line) in the plane $x = 0$. Field strengths are given in relativistic units.

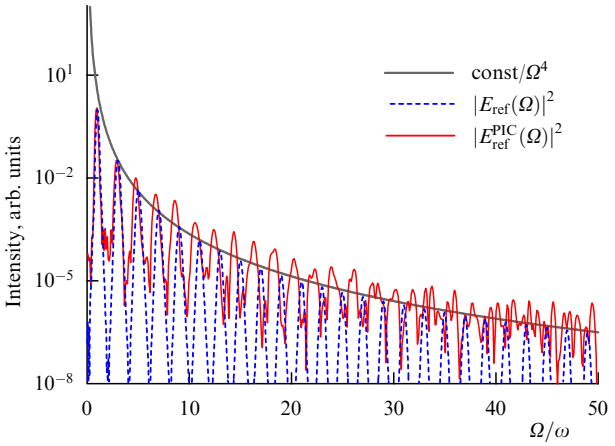

Figure 11. Spectrum of the reflected field shown in Fig. 10 and approximation of the envelope of the spectrum.

jumps. These are just those jumps from which one can produce short pulses by filtering out the low-frequency components of the field.

Figure 11 displays the spectrum of the reflected field $|\hat{E}_{\rm ref}(\Omega)|^2$ calculated numerically. The envelope of the spectrum is well approximated by

$$\left|E_{\rm ref}^{\rm appr}(\Omega)\right|^2 = 30\left(\frac{\Omega}{\omega}\right)^{-4}\left(\frac{an_{\rm cr}}{N_{\rm e}}\right)^2|\hat{E}_{\rm inc}|^2\,, \qquad (44)$$

where $n_{\rm cr} = m\omega^2/(4\pi e^2)$ is the critical plasma density, and $\hat{E}_{\rm inc}$ is the Fourier amplitude of the incident field $E_{\rm inc}(t)$ at frequency ω.

Our calculations give evidence that, at least in the parameter range of $10^{23}\ {\rm cm}^{-3} \leqslant N_{\rm e} \leqslant 6\times10^{23}\ {\rm cm}^{-3}$ and $1\times(N_{\rm e}\times10^{-23}\ {\rm cm}^3) \leqslant a \leqslant 15\times(N_{\rm e}\times10^{-23}\ {\rm cm}^3)$, the values of the square of the amplitude for odd harmonics of order from 5 to 50 predicted by this formula differ little (by no more than twice) from those given by $|\hat{E}_{\rm ref}(\Omega)|^2$. They are proportional to the square of the intensity of the driving field and inversely proportional to the square of the plasma density. The conversion efficiency $|E_{\rm ref}^{\rm appr}(\Omega)|^2/|\hat{E}_{\rm inc}|^2$ is inversely proportional to the square of the similarity parameter $S = N_{\rm e}/n_{\rm cr}a$ introduced in Ref. [211]. Figures 10 and 11 also give the results of PIC simulations. They are qualitatively consistent with the results of calculations based on the model adopted here. It is worth noting that the relationship $|\hat{E}_{\rm ref}(\Omega)|^2 \sim (\Omega/\omega)^{-q}$ was obtained more than once in the analytical models. It also appears that different models give different values for the exponent q: 5/2 [212], 8/3 [213], 2 [214], and others. PIC simulations indicate that the index q decreases (in absolute value) with decreasing plasma density or with increasing light intensity. The numerical model applied here is based on assumptions which are more valid for higher plasma density and become inadequate for both very large and very low (subrelativistic) radiation intensities.

Figure 12 demonstrates a train of attosecond pulses obtained from the field $E_{\rm ref}(t)$, shown in Fig. 10, through spectral filtering described by the formula

$$E_{\rm filt}(t) = \frac{1}{2\pi}\int_{\Omega_1}^{\Omega_2}\exp\left(-{\rm i}\Omega t\right){\rm d}\Omega \times\int_{-\infty}^{\infty}\exp\left({\rm i}\Omega\tau\right)E_{\rm ref}(\tau)\,{\rm d}\tau + {\rm c.c.}, \qquad (45)$$

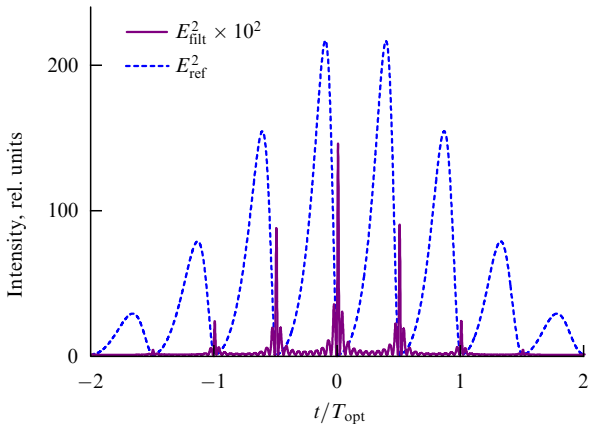

Figure 12. Square of the reflected field calculated using relationship (42) before filtering (dashed line, just as in Fig. 10) and after spectral filtering using formula (45) with $\Omega_1 = 10\omega$ and $\Omega_2 = 50\omega$ (thick solid line). Field intensities are given in relativistic units.

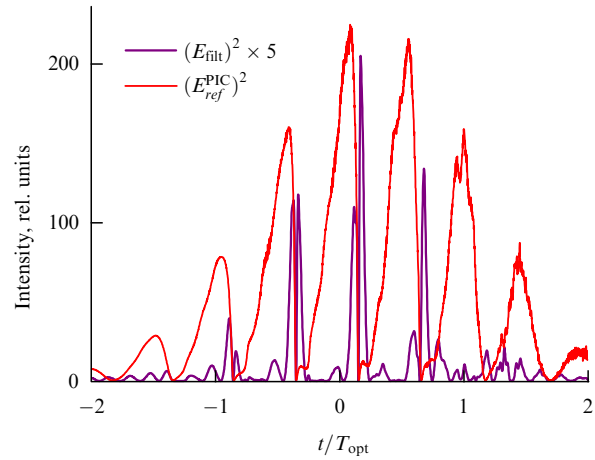

Figure 13. Square of the reflected field calculated by the PIC method before filtering (thin solid line, just as in Fig. 10) and after spectral filtering using formula (45) with $\Omega_1 = 4\omega$ and $\Omega_2 = 50\omega$ (thick solid line). Field intensities are given in relativistic units.

with $\Omega_1 = 10\omega$ and $\Omega_2 = 50\omega$. Attosecond pulses appear synchronously with the jumps of the field $E_{\rm ref}(t)$.

It should be emphasized that, even when the duration of the driving pulse [i.e., FWHM of envelope $E_{\rm inc}^2(t)$] is equal to two cycles of the field, the central AP significantly exceeds in amplitude the adjacent pulses. In the oblique incidence case, the pulses closest to the central AP disappear (see below).

Figure 13 demonstrates the train of APs separated by spectral filtering (45) of the field, shown in Fig. 10, being calculated by the PIC method. Qualitatively, it is close to the train represented in Fig. 12.

Thus, for the parameters invoked above, AP generation can be described well in the framework of the proposed model. However, the field intensities on the order of $10^{20}\ {\rm W\ cm}^{-2}$ considered here have not yet been reached for such a short pulse. Furthermore, the plasma density used above is unrealistically small. Indeed, the plasma parameters relevant to equation (41) correspond to $N_{\rm e}/n_{\rm cr} \approx 60$. Let us estimate the value of this ratio in a real experiment. At relativistic intensities, a deep and fast ionization of the medium occurs. It proceeds in the barrier suppression regime if the electric field strength exceeds $U^2/4Ze^3$, where

U is the ionization potential, and Z is the charge of the atomic core [215]. Estimates show that, for instance, for quartz irradiated with an intensity of 10^{20} W cm^{-2}, barrier-suppression ionization involves almost all the electrons (except K-electrons of silicon). Upon complete ionization of the target, the plasma density is close to $3\times10^{23}\rho$ per g, where ρ is the mass density, so that, for example, with $\lambda = 0.75$ μm and $\rho = 2$ g cm^{-3}, we obtain $N_e/n_{cr} \approx 300$.

3.3.2 Oblique incidence. Sharp plasma–vacuum boundary. Not only is the transition from normal to oblique incidence technically convenient; it also leads to a significant increase in the AP amplitude and simplifies the selection of a single AP from the train. At oblique incidence of p-polarized light, the electric field comprises a component normal to the target surface, which oscillates at the fundamental frequency, whereas the Lorentz force is always directed into the target and oscillates at the doubled frequency. In one half-cycle, this component of the field enhances light pressure on the electron component of the plasma, whereas in the other half-cycle it contributes (together with the potential field) to electron acceleration in the direction opposite to the beam propagation. As a result, the AP amplitude increases and the repetition frequency is one half that of normal incidence (with large angles of incidence, only those APs survive which are generated in the half-cycle in which the electric field of the wave is directed into the plasma).

For illustration, Figs 14 and 15 display, respectively, the reflected field and its spectrum calculated using PIC code for the case of an obliquely incident sinusoidal pulse similar to that given by formula (43), with a 2.5-cycle duration, intensity $I = 100I_{rel}$, and incidence angle $\pi/5$ with respect to the surface of a plasma with density $N_e = 100n_{cr}$.

The results of calculations performed for different intensities of a 2-cycle Gaussian pulse incident at angle $\pi/5$ on the plasma with a density one hundred times the critical density are listed in Table 1. The middle column shows the intensity of APs extracted from the reflected field by spectral filtering [see formula (45)], with $\Omega_1 = 5\omega$ and $\Omega_2 = 45\omega$; the right-hand column demonstrates the contrast of the most intense APs with respect to adjacent pulses in the train. At driving pulse intensities below $40I_{rel}$, APs with a contrast greater than two were not observed.

3.3.3 Oblique incidence. Smooth plasma–vacuum boundary. HHG efficiency increases significantly as one proceeds from a sharp plasma–vacuum boundary case to the case of a smoother plasma density distribution [216]. The reason for the high efficiency of the laser light–plasma interaction in the latter case consists presumably in the fact that this interaction occurs mainly in a quasiresonance region with a plasma density slightly higher than the critical density.

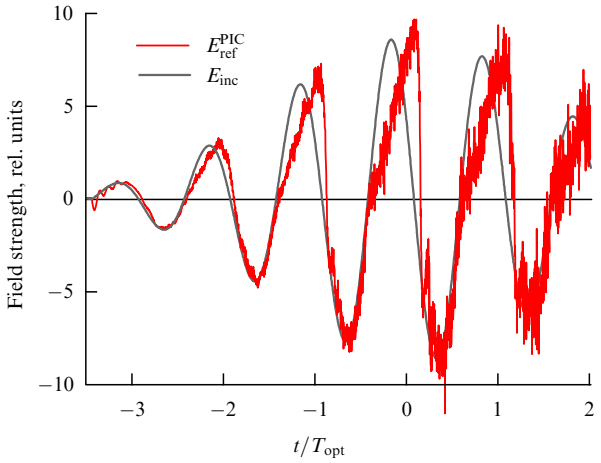

Figure 14. (Color online.) Incident (gray line) and reflected (thin red line) field calculated by the PIC method. Field strengths are given in relativistic units.

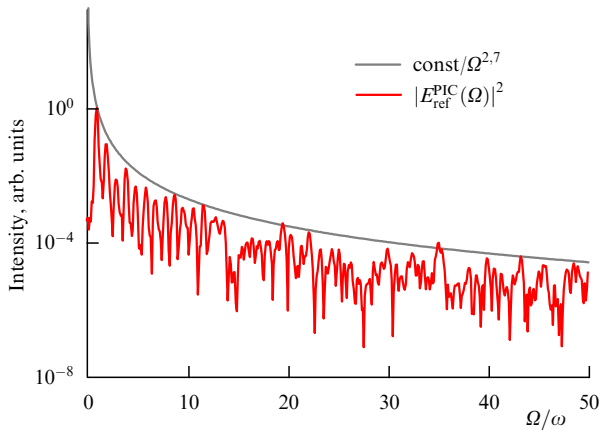

Figure 15. (Color online.) Spectrum of the reflected field shown in Fig. 14, and approximation of the envelope of the spectrum.

It turns out that the case of oblique incidence on a plasma with a smooth boundary is the most favorable in this regard. Below, we discuss the results of calculations carried out for the following distribution of the plasma density: for $x < 0$, the initial density is zero; within the interval $0-8L$ it grows exponentially as $N_e = N_{max}\exp(x/L - 8)$ (below, the parameter L is called the gradient length), and for $x \geqslant 8L$ the density is equal to N_{max}.

Table 2 lists the results of calculations performed for the case of a 2-cycle laser pulse incident at angle $2\pi/15$ on the surface of a plasma with $N_{max} = 200n_{cr}$ and gradient length of $L = 0.064\lambda$.

These results indicate that in the experiments with an oblique incidence of light on the plasma with a smoothly

Table 1.

Driving pulse intensity, relativistic units	Intensity of AP, relativistic units; $\Omega_1 = 5\omega$, $\Omega_2 = 45\omega$	Contrast
200	85	4.6
160	67	6.8
120	34	3.75
80	9.6	3.3
50	2.54	2.7

Table 2.

Driving pulse intensity, relativistic units	Range of spectral filtering $(\Omega_1 - \Omega_2)/\omega$	Intensity of AP, relativistic units	Contrast
40	5–60	37.9	2.85
20	5–60	19.6	2.2
5	5–30	3.5	4.6
2.5	5–30	0.6	3.5

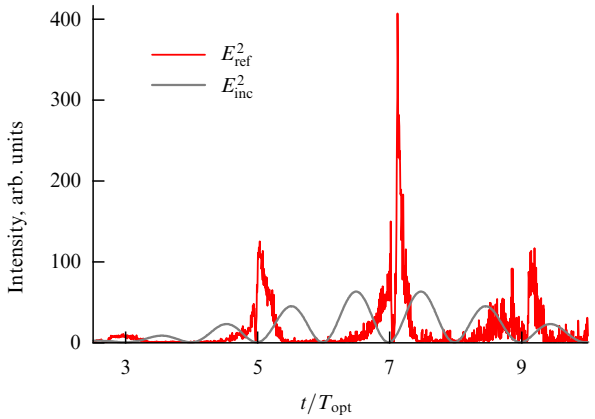

Figure 16. (Color online.) Square of the field of the incident (thick line) and reflected (thin red line) radiation.

varying density, APs with relatively high contrast and intensity can be obtained utilizing driving light with an intensity an order of magnitude lower than in the case of plasma having a sharp boundary.

For slightly larger angles of incidence and driving beam intensities, it turns out that the pulse reflected from a plasma with a smoothly varying density breaks up into a train of short pulses whose duration falls within the attosecond range without any spectral filtering, and their intensity is significantly higher than that of the incident (driving) pulse. Figure 16 plots such an AP train obtained in the calculation with $L = 0.064\lambda$, $N_{max} = 100n_{cr}$, and the angle of incidence $\pi/5$; the incident pulse is given by expression (43) with $a = 10$. The duration of the central pulse in the reflected AP train is approximately 30 times shorter than the period of the incident light; the contrast with respect to the adjacent pulses is about 3.25.

The results of numerical simulations show that in the range of $L \in [0; 0.3\lambda]$ the intensity ratio I_{ref}/I_{inc} of the reflected and incident pulses increases and the AP duration decreases with increasing the gradient length.

Both the methods and the capability of preparing flat plasma layers with relatively large gradient lengths ($L \sim 0.1\lambda$) and controlled parameters are independent issues which have not yet been considered in detail. The creation and utilization of such layers may be significantly hampered by the instabilities arising during the expansion of a dense plasma. Notice, however, that, as the research implies, an efficient AP generation with driving pulses of ultrarelativistic intensity can be achieved in the cases of both a smooth (with a gradient length L on the order of a few tenths of λ) and a sharp ($L = 0$) plasma–vacuum interface. In particular, making some model assumptions the authors of Ref. [206] concluded against the possibility of obtaining a large value of the ratio $I_{ref}/I_{inc} \gg 1$ with a stepwise profile of the plasma density. Calculations give evidence that for L in the range of 0 to 0.8λ, the above ratio can significantly exceed unity [204] and the emission spectra may exhibit a slow decay with a harmonic order [205] characteristic of the coherent synchrotron emission mechanism.

3.4 Concluding remarks

Summing up this section, we point out a number of studies which have explored various configurations of the plasma targets and driving light for producing APs on a plasma surface.

AP generation in the interaction of intense laser pulses with thin plasma layers having a rectangular density profile was studied in Refs [214, 217]. The results of simulations (using the PIC method) have revealed the feasibility of producing a high-contrast isolated APs if certain strict requirements on the intensity of the driving light or the thickness of the layer are met. According to the findings [217], the intensity should be comparable with some critical value

$$I_{cr} = I_{rel}\left(\frac{\pi l}{\lambda}\frac{N_e}{n_{cr}}\right)^2,$$

where l is the thickness of the layer (at an intensity exceeding I_{cr}, the plasma layer is destroyed).

In Refs [218, 219], a method of producing an isolated AP was proposed, based on the application of tight focusing of the driving laser beam, providing a plasma surface deformation which entails, in turn, both scanning the angle of reflection of the radiation and focusing it. The simulations [218, 219] involved relatively low plasma densities and laser intensities (on the order of $10I_{rel}$). It seems likely that, when working with real targets, the intensity requirements will become much more severe.

In Ref. [220], a mechanism was proposed for AP generation with the driving radiation composed of a fundamental field and its second harmonic. It has been demonstrated that under certain conditions a 5% conversion of the fundamental field into the second harmonic leads to an increase in the intensity of the generated isolated AP by an order of magnitude.

In paper [221], a more complex method of isolated AP generation was elaborated, which is based on making use the two beams with different intensities, polarizations, and frequencies.

In recent years, a number of experimental groups have made significant progress in obtaining relativistically intense pulses of short duration and high contrast (see, e.g., Refs [201, 222]), suitable for experiments on the generation of high-order harmonics and APs on the surface. Analysis indicates that the parameters of the laser pulses obtained in these studies do not yet provide the possibility of producing isolated APs in experiments with plasmas having a sharp boundary and high density. It is expected that in the coming years few-cycle optical pulses with significantly higher power and shorter duration will be available. Isolated AP generation may also benefit from the employment of targets made of low-density materials, such as polymethacrylate. Naturally, it would be extremely useful to engineer controllable plasma layers with a large gradient length (about a few tenths of the laser radiation wavelength).

Finally, we note also that there are discussions of the possibility of AP generation in the interaction of a laser field of ultrarelativistic intensity with *rarefied* plasmas [223, 224].

4. Conclusion

In this review, two approaches to AP production are considered, which make use of the interaction of moderately intense (about 10^{14} W cm^{-2}) radiation with gaseous media and the interaction of ultrarelativistically intense laser radiation with a dense plasma. The first of these approaches has been explored in great detail to date. At the same time, active theoretical research in this direction continues nowa-

days and is focused on issues such as resonance-enhanced HHG, relativistic effects in HHG, harmonic generation in molecular gases and crystals, and HHG in fields containing components of different frequencies and polarizations.

HHG remains the only well-studied nonlinear high-order *optical* process. Great progress can be expected to come soon in the research on other nonlinear optical processes of a high order; for instance, the results of experimental [225] and numerical [226] research were published recently, which were interpreted by the authors as the demonstration of multiphoton parametric amplification in the UV region; this became the subject of a lively discussion [227–229]. The study of purely optical multiphoton processes opens the way to the development of nonperturbative nonlinear optics [230]. The generation and amplification of coherent ultraviolet radiation on the basis of these processes may lead to new methods of producing intense APs in gaseous media.

Ways of producing APs without utilizing HHG are also discussed, in particular:

(i) summation of many anti-Stokes components generated by stimulated Raman scattering [231–233]. The advantages of this method are the relatively high efficiency of generation and, therefore, high energy (at the level of a few microjoules) of the generated UV radiation, whereas the drawback is a much narrower, compared to the HHG case, spectral band in which the anti-Stokes components of comparable intensity are generated, resulting in a rather long pulse duration (about 1 fs) of the generated UV radiation;

(ii) resonant generation of in-phase spectral components in the process of the interaction of vacuum ultraviolet or X-ray radiation with the atoms in a gas simultaneously irradiated by an intense laser field, which causes quasistatic ionization of excited atomic states and/or a shift of excited energy levels [234, 235]. This method implies the availability of a source of narrow-band high-frequency radiation. One of the advantages of the method consists in the originally present synchronization of the spectral components, which allows AP production [236]. A similar approach was applied in an experiment on the formation of time-bin qubits and pulse sequences from single γ-ray photons [237].

Theoretical studies of AP generation in the interaction of laser radiation with dense plasmas are based mainly on numerical simulations employing the PIC method. For a qualitative analysis of the phenomenon, several models were constructed which have different ranges of applicability. In this review, we presented the theory built around the oscillating mirror model; this theory provides good quantitative agreement with the numerical results in a certain range of parameters.

On the basis of both numerical and simple model calculations, it can be concluded that the APs produced via reflection of a laser pulse from the dense plasma boundary can be of much higher energy than those generated in gases. However, such a method for producing APs is much more complex from the experimental point of view, since it requires both high intensity and high contrast of the driving pulse, which makes it difficult to fabricate on this basis devices for practical use in attosecond physics. Recent advances in the production, measurement, and applications of APs relate mainly to attosecond pulses generated in gas media.

This study was partially supported by the Russian Foundation for Basic Research (grant Nos 14-02-00762-a, 16-02-00858-a, and 14-02-00878-a).

References

1. Keldysh L V *Sov. Phys. JETP* **20** 1307 (1965); *Zh. Eksp. Teor. Fiz.* **47** 1945 (1964)
2. Ackermann W et al. *Nature Photon.* **1** 336 (2007)
3. Emma P et al. *Nature Photon.* **4** 641 (2010)
4. Ishikawa T et al. *Nature Photon.* **6** 540 (2012)
5. Allaria E et al. *Nature Photon.* **6** 699 (2012)
6. Mitzner R et al. *Opt. Express* **16** 19909 (2008)
7. Lambert G et al. *Nature Phys.* **4** 296 (2008)
8. Ackermann S et al. *Phys. Rev. Lett.* **111** 114801 (2013)
9. McPherson A et al. *J. Opt. Soc. Am. B* **4** 595 (1987)
10. Ferray M et al. *J. Phys. B* **21** L31 (1988)
11. Li X F et al. *Phys. Rev. A* **39** 5751 (1989)
12. Sarukura N et al. *Phys. Rev. A* **43** 1669(R) (1991)
13. Crane J K et al. *Opt. Lett.* **17** 1256 (1992)
14. Miyazaki K, Sakai H *J. Phys. B* **25** L83 (1992)
15. L'Huillier A, Balcou Ph *Phys. Rev. Lett.* **70** 774 (1993)
16. Macklin J J, Kmetec J D, Gordon C L (III) *Phys. Rev. Lett.* **70** 766 (1993)
17. Platonenko V T, Strelkov V V *Quantum Electron.* **28** 564 (1998); *Kvantovaya Elektron.* **25** 582 (1998)
18. Winterfeldt C, Spielmann C, Gerber G *Rev. Mod. Phys.* **80** 117 (2008)
19. Chang Z et al. *Phys. Rev. Lett.* **79** 2967 (1997)
20. Spielmann Ch et al. *Science* **278** 661 (1997)
21. Seres J et al. *Nature* **433** 596 (2005)
22. Silin V P *Sov. Phys. JETP* **20** 1510 (1965); *Zh. Eksp. Teor. Fiz.* **47** 2254 (1964)
23. Silin V P *JETP* **87** 468 (1998); *Zh. Eksp. Teor. Fiz.* **114** 864 (1998)
24. Carman R L, Rhodes C K, Benjamin R F *Phys. Rev. A* **24** 2649 (1981)
25. Tuebner U, Gibbon P *Rev. Mod. Phys.* **81** 445 (2009)
26. Thaury C, Quéré F *J. Phys. B* **43** 213001 (2010)
27. Dromey B et al. *Phys. Rev. Lett.* **99** 085001 (2007)
28. Nomura Y et al. *Nature Phys.* **5** 124 (2009)
29. Hörlein R et al. *New J. Phys.* **12** 043020 (2010)
30. Wheeler J A et al. *Nature Photon.* **6** 829 (2012)
31. Krause J L, Schafer K J, Kulander K C *Phys. Rev. Lett.* **68** 3535 (1992)
32. Schafer K J et al. *Phys. Rev. Lett.* **70** 1599 (1993)
33. Corkum P B *Phys. Rev. Lett.* **71** 1994 (1993)
34. Gladkov S M, Koroteev N I *Sov. Phys. Usp.* **33** 554 (1990); *Usp. Fiz. Nauk* **160** (7) 105 (1990)
35. Kuchiev M Yu *JETP Lett.* **45** 404 (1987); *Pis'ma Zh. Eksp. Teor. Fiz.* **45** 319 (1987)
36. Brunel F *J. Opt. Soc. Am. B* **7** 521 (1990)
37. Becker W et al. *Adv. At. Mol. Opt. Phys.* **48** 35 (2002)
38. Paulus G G, Becker W, Walther H *Phys. Rev. A* **52** 4043 (1995)
39. Farkas Gy, Tóth Cs *Phys. Lett. A* **168** 447 (1992)
40. Krause J L, Schafer K J, Kulander K C *Phys. Rev. A* **45** 4998 (1992)
41. Cormier E, Lambropoulos P *J. Phys. B* **30** 77 (1997)
42. Tong X M, Chu S I *Chem. Phys.* **217** 119 (1997)
43. Bauer D, Mulser P *Phys. Rev. A* **59** 569 (1999)
44. Muller H G *Phys. Rev. A* **60** 1341 (1999)
45. Strelkov V V et al. *J. Phys. B* **39** 577 (2006)
46. Popov A M, Tikhonova O V, Volkova E A *Laser Phys.* **21** 1593 (2011)
47. Gonoskov A A, Gonoskov I A, physics/0607120
48. Strelkov V V et al. *Phys. Rev. A* **86** 013404 (2012)
49. Fleck J A, Jr, Morris J R, Feit M D *Appl. Phys.* **10** 129 (1976)
50. Strelkov V V et al. *Phys. Rev. Lett.* **107** 043902 (2011)
51. Emelin M Yu, Ryabikin M Yu, Sergeev A M *New J. Phys.* **10** 025026 (2008)
52. Lewenstein M et al. *Phys. Rev. A* **49** 2117 (1994)
53. Fedorov M V, Peatross J *Phys. Rev. A* **52** 504 (1995)
54. Antoine Ph et al. *Phys. Rev. A* **55** 1314 (1997)
55. Kuchiev M Yu, Ostrovsky V N *Phys. Rev. A* **60** 3111 (1999)
56. Platonenko V T *Quantum Electron.* **31** 55 (2001); *Kvantovaya Elektron.* **31** 55 (2001)
57. Platonenko V T, Sterjantov A F *Quantum Electron.* **36** 1074 (2006); *Kvantovaya Elektron.* **36** 1074 (2006)

58. Emelin M Yu, Ryabikin M Yu, Sergeev A M *JETP* **106** 203 (2008); *Zh. Eksp. Teor. Fiz.* **133** 243 (2008)
59. Pérez-Hernández J A, Roso L, Plaja L *Opt. Express* **17** 9891 (2009)
60. Frolov M V et al. *J. Phys. B* **42** 035601 (2009)
61. Emelin M Yu, Ryabikin M Yu, Sergeev A M *Opt. Express* **18** 2269 (2010)
62. Kan C et al. *Phys. Rev. A* **52** R4336 (1995)
63. Gaarde M B et al. *Phys. Rev. A* **59** 1367 (1999)
64. Khokhlova M A, Strelkov V V *Phys. Rev. A* **93** 043416 (2016)
65. Becker W, Long S, McIver J K *Phys. Rev. A* **50** 1540 (1994)
66. Antoine Ph et al. *Phys. Rev. A* **53** 1725 (1996)
67. Becker W et al. *Phys. Rev. A* **56** 645 (1997)
68. Lewenstein M, Salières P, L'Huillier A *Phys. Rev. A* **52** 4747 (1995)
69. Paulus G G et al. *Phys. Rev. Lett.* **84** 3791 (2000)
70. Salières P et al. *Science* **292** 902 (2001)
71. Milošević D B, Bauer D, Becker W *J. Mod. Opt.* **53** 125 (2006)
72. Goreslavskii S P, Popruzhenko S V *JETP Lett.* **68** 902 (1998); *Pis'ma Zh. Eksp. Teor. Fiz.* **68** 858 (1998)
73. Goreslavskii S P, Popruzhenko S V *JETP* **90** 778 (2000); *Zh. Eksp. Teor. Fiz.* **117** 895 (2000)
74. Goreslavski S P et al. *Phys. Rev. Lett.* **93** 233002 (2004)
75. Bauer D, Milošević D B, Becker W *J. Mod. Opt.* **53** 135 (2006)
76. Bauer D *Phys. Rev. Lett.* **94** 113001 (2005)
77. Ivanov M Yu, Brabec Th, Burnett N *Phys. Rev. A* **54** 742 (1996)
78. Strelkov V V *Phys. Rev. A* **74** 013405 (2006)
79. Landau L D, Lifshitz E M *Quantum Mechanics. Non-Relativistic Theory* (Oxford: Pergamon Press, 1977); Translated from Russian: *Kvantovaya Mekhanika. Nerelyativistskaya Teoriya* (Moscow: Nauka, 1989)
80. Boge R et al. *Phys. Rev. Lett.* **111** 103003 (2013)
81. Landsman A S, Keller U *Phys. Rep.* **547** 1 (2015)
82. Perelomov A M, Popov V S, Terent'ev M V *Sov. Phys. JETP* **23** 924 (1966); *Zh. Eksp. Teor. Fiz.* **50** 1393 (1966)
83. Perelomov A M, Popov V S, Terent'ev M V *Sov. Phys. JETP* **24** 207 (1967); *Zh. Eksp. Teor. Fiz.* **51** 309 (1966)
84. Perelomov A M, Popov V S *Sov. Phys. JETP* **25** 336 (1967); *Zh. Eksp. Teor. Fiz.* **52** 514 (1967)
85. Popov V S *Phys. Usp.* **47** 855 (2004); *Usp. Fiz. Nauk* **174** 921 (2004)
86. Strelkov V V, Platonenko V T, Becker A *Phys. Rev. A* **71** 053808 (2005)
87. Antoine Ph, L'Huillier A, Lewenstein M *Phys. Rev. Lett.* **77** 1234 (1996)
88. Platonenko V T, Strelkov V V *Quantum Electron.* **27** 779 (1997); *Kvantovaya Elektron.* **24** 799 (1997)
89. Gaarde M B, Schafer K J *Phys. Rev. A* **65** 031406(R) (2002)
90. Alexandrov L N, Emelin M Yu, Ryabikin M Yu *J. Phys. B* **47** 204028 (2014)
91. Ilyakov I E et al. *JETP Lett.* **101** 74 (2015); *Pis'ma Zh. Eksp. Teor. Fiz.* **101** 78 (2015)
92. Velotta R et al. *Phys. Rev. Lett.* **87** 183901 (2001)
93. Lein M et al. *Phys. Rev. Lett.* **88** 183903 (2002)
94. Lein M et al. *Phys. Rev. A* **66** 023805 (2002)
95. Emelin M Yu et al. *JETP Lett.* **77** 212 (2003); *Pis'ma Zh. Eksp. Teor. Fiz.* **77** 254 (2003)
96. Gonoskov I A, Ryabikin M Yu, Sergeev A M *J. Phys. B* **39** S445 (2006)
97. Bandrauk A D, Chelkowski S, Lu H *J. Phys. B* **42** 075602 (2009)
98. Boutu W et al. *Nature Phys.* **4** 545 (2008)
99. Zhou X et al. *Phys. Rev. Lett.* **102** 073902 (2009)
100. Moreno P, Plaja L, Roso L *Phys. Rev. A* **55** R1593 (1997)
101. Bandrauk A D, Yu H *Phys. Rev. A* **59** 539 (1999)
102. Mairesse Y et al. *Phys. Rev. Lett.* **104** 213601 (2010)
103. Kreibich T et al. *Phys. Rev. Lett.* **87** 103901 (2001)
104. Lein M *Phys. Rev. Lett.* **94** 053004 (2005)
105. Baker S et al. *Science* **312** 424 (2006)
106. Lein M *J. Phys. B* **40** R135 (2007)
107. Haessler S, Caillat J, Salières P *J. Phys. B* **44** 203001 (2011)
108. Zhou X X et al. *Phys. Rev. A* **71** 061801(R) (2005)
109. Chirilă C C, Lein M *Phys. Rev. A* **73** 023410 (2006)
110. Madsen C B, Madsen L B *Phys. Rev. A* **74** 023403 (2006)
111. Parker J S et al. *J. Phys. B* **33** 1057 (2000)
112. Taylor K T et al. *Eur. Phys. J. D* **26** 67 (2003)
113. Taylor K T et al. *J. Mod. Opt.* **54** 1959 (2007)
114. Popov A M, Tikhonova O V, Volkova E A *Laser Phys.* **17** 103 (2007)
115. Volkova E A, Popov A M, Tikhonova O V *Opt. Spectrosc.* **102** 159 (2007); *Opt. Spektrosk.* **102** 192 (2007)
116. Nepstad R, Birkeland T, Førre M *Phys. Rev. A* **81** 063402 (2010)
117. Itatani J et al. *Nature* **432** 867 (2004)
118. Morishita T et al. *Phys. Rev. Lett.* **100** 013903 (2008)
119. Frolov M V et al. *Phys. Rev. Lett.* **102** 243901 (2009)
120. Frolov M V et al. *Phys. Rev. A* **83** 043416 (2011)
121. Wörner H J et al. *Phys. Rev. Lett.* **102** 103901 (2009)
122. Higuet J et al. *Phys. Rev. A* **83** 053401 (2011)
123. Farrell J P et al. *Phys. Rev. A* **83** 023420 (2011)
124. Rothhardt J et al. *Phys. Rev. Lett.* **112** 233002 (2014)
125. Shiner A D et al. *Nature Phys.* **7** 464 (2011)
126. Oleinikov P A, Platonenko V T, Ferrante G *JETP Lett.* **60** 246 (1994); *Pis'ma Zh. Eksp. Teor. Fiz.* **60** 235 (1994)
127. Plaja L, Roso L *J. Mod. Opt.* **40** 793 (1993)
128. de Morisson Faria C F et al. *Phys. Rev. A* **65** 023404 (2002)
129. Taïeb R et al. *Phys. Rev. A* **68** 033403 (2003)
130. Ganeev R A *Phys. Usp.* **56** 772 (2013); *Usp. Fiz. Nauk* **183** 815 (2013)
131. Milošević D B *J. Phys. B* **40** 3367 (2007)
132. Strelkov V *Phys. Rev. Lett.* **104** 123901 (2010)
133. Frolov M V, Manakov N L, Starace A F *Phys. Rev. A* **82** 023424 (2010)
134. Strelkov V V, Khokhlova M A, Shubin N Yu *Phys. Rev. A* **89** 053833 (2014)
135. Tudorovskaya M, Lein M *Phys. Rev. A* **84** 013430 (2011)
136. Shen Y R *The Principles of Nonlinear Optics* (New York: J. Wiley, 1984); Translated into Russian: *Printsipy Nelineinoi Optiki* (Moscow: Nauka, 1989)
137. Akhmanov S A, Khokhlov R V *Problemy Nelineinoi Optiki* (*Elektromagnitnye Volny v Nelineinykh Dispergiruyushchikh Sredakh)* (Problems of Nonlinear Optics (Electromagnetic Waves in Nonlinear Dispersive Media)) (Ser. Progress in Science, 1961 – 1963) (Moscow: VINITI AN SSSR, 1964)
138. Salières P, L'Huillier A, Lewenstein M *Phys. Rev. Lett.* **74** 3776 (1995)
139. Peatross J, Fedorov M V, Kulander K C *J. Opt. Soc. Am. B* **12** 863 (1995)
140. Peatross J, Meyerhofer D D *Phys. Rev. A* **52** 3976 (1995)
141. Balcou Ph et al. *Phys. Rev. A* **55** 3204 (1997)
142. Platonenko V T, Strelkov V V *Quantum Electron.* **30** 236 (2000); *Kvantovaya Elektron.* **30** 236 (2000)
143. Zaïr A et al. *Phys. Rev. Lett.* **100** 143902 (2008)
144. Strelkov V V, Doctoral Thesis of Phys.-Math. Sci. (Moscow: Prokhorov General Physics Institute RAS, 2009)
145. Platonenko V T, Strelkov V V, Ferrante G *J. Opt. Soc. Am. B* **19** 1611 (2002)
146. Platonenko V T, Strelkov V V, Ferrante G *Laser Phys.* **12** 888 (2002)
147. Batebi S, Platonenko V T *Quantum Electron.* **34** 71 (2004); *Kvantovaya Elektron.* **34** 71 (2004)
148. Rundquist A et al. *Science* **280** 1412 (1998)
149. Constant E et al. *Phys. Rev. Lett.* **82** 1668 (1999)
150. Durfee C G (III) et al. *Phys. Rev. Lett.* **83** 2187 (1999)
151. Popmintchev T et al. *Science* **336** 1287 (2012)
152. Lange H R et al. *Phys. Rev. Lett.* **81** 1611 (1998)
153. Christov I P, Kapteyn H C, Murnane M M *Opt. Express* **7** 362 (2000)
154. Paul A et al. *Nature* **421** 51 (2003)
155. Birulin A V, Platonenko V T, Strelkov V V *Quantum Electron.* **26** 377 (1996); *Kvantovaya Elektron.* **23** 387 (1996)
156. Birulin A V, Platonenko V T, Strelkov V V *JETP* **83** 33 (1996); *Zh. Eksp. Teor. Fiz.* **110** 63 (1996)
157. Heyl C M et al. *Phys. Rev. Lett.* **112** 143902 (2014)
158. Hickstein D D *Nature Photon.* **9** 743 (2015)
159. Zepf M et al. *Phys. Rev. Lett.* **99** 143901 (2007)
160. Seres J et al. *Nature Phys.* **3** 878 (2007)
161. Tosa V, Yakovlev V S, Krausz F *New J. Phys.* **10** 025016 (2008)
162. Popmintchev T et al. *Nature Photon.* **4** 822 (2010)
163. Gaarde M B, Tate J L, Schafer K J *J. Phys. B* **41** 132001 (2008)
164. Kazamias S et al. *Phys. Rev. Lett.* **90** 193901 (2003)
165. Strelkov V V, Mével E, Constant E *New J. Phys.* **10** 083040 (2008)
166. Jullien A et al. *Appl. Phys. B* **93** 433 (2008)
167. Geissler M, Tempea G, Brabec T *Phys. Rev. A* **62** 033817 (2000)

168. Tempea G et al. *Phys. Rev. Lett.* **84** 4329 (2000)
169. Vozzi C et al. *Opt. Lett.* **32** 2957 (2007)
170. Gu X et al. *Opt. Express* **17** 62 (2009)
171. Hauri C P et al. *Opt. Lett.* **32** 868 (2007)
172. Schmidt B E et al. *Appl. Phys. Lett.* **96** 121109 (2010)
173. Andriukaitis G et al. *Opt. Lett.* **36** 2755 (2011)
174. Deng Y et al. *Opt. Lett.* **37** 4973 (2012)
175. Sheehy B et al. *Phys. Rev. Lett.* **83** 5270 (1999)
176. Shan B, Chang Z *Phys. Rev. A* **65** 011804(R) (2001)
177. Takahashi E J et al. *Phys. Rev. Lett.* **101** 253901 (2008)
178. Emelina A S, Emelin M Yu, Ryabikin M Yu *Quantum Electron.* **44** 470 (2014); *Kvantovaya Elektron.* **44** 470 (2014)
179. Kim A V, Ryabikin M Yu, Sergeev A M *Phys. Usp.* **42** 54 (1999); *Usp. Fiz. Nauk* **169** 58 (1999)
180. Taranukhin V D *Laser Phys.* **10** 330 (2000)
181. Chirilă C C et al. *Phys. Rev. A* **66** 063411 (2002)
182. Emelina A S, Emelin M Yu, Ryabikin M Yu *J. Opt. Soc. Am. B* **32** 2478 (2015)
183. Platonenko V T, Sterjantov A F, Strelkov V V *Laser Phys.* **13** 443 (2003)
184. Tate J et al. *Phys. Rev. Lett.* **98** 013901 (2007)
185. Schiessl K et al. *Phys. Rev. Lett.* **99** 253903 (2007)
186. Gordon A, Kärtner F X *Opt. Express* **13** 2941 (2005)
187. Frolov M V, Manakov N L, Starace A F *Phys. Rev. Lett.* **100** 173001 (2008)
188. Colosimo P et al. *Nature Phys.* **4** 386 (2008)
189. Shiner A D et al. *Phys. Rev. Lett.* **103** 073902 (2009)
190. Doumy G et al. *Phys. Rev. Lett.* **102** 093002 (2009)
191. Popmintchev T et al. *Proc. Natl. Acad. Sci. USA* **106** 10516 (2009)
192. Yakovlev V S, Ivanov M, Krausz F *Opt. Express* **15** 15351 (2007)
193. Sola I et al. *Nature Phys.* **2** 319 (2006)
194. Vozzi C et al. *Phys. Rev. Lett.* **95** 153902 (2005)
195. Kanai T, Minemoto S, Sakai H *Nature* **435** 470 (2005)
196. Torres R et al. *Opt. Express* **18** 3174 (2010)
197. Grigor'ev Yu N, Vshivkov V A, Fedoruk M P *Chislennoe Modelirovanie Metodami Chastits-v-Yacheikakh* (Numerical Simulation by Particle-in-Cell Methods) (Novosibirsk: Izd. SO RAN, 2004)
198. Birdsall C K, Langdon A B *Plasma Physics, via Computer Simulation* (New York: McGraw-Hill, 1984); Translated into Russian: *Fizika Plazmy i Chislennoe Modelirovanie* (Moscow: Energoatomizdat, 1989)
199. Quéré F et al. *Phys. Rev. Lett.* **96** 125004 (2006)
200. Brunel F *Phys. Rev. Lett.* **59** 52 (1987)
201. Thaury C et al. *Nature Phys.* **3** 424 (2007)
202. Tarasevitch A et al. *Phys. Rev. Lett.* **98** 103902 (2007)
203. Bulanov S V, Naumova N M, Pegoraro F *Phys. Plasmas* **1** 745 (1994)
204. Van der Brügge D, Pukhov A *Phys. Plasmas* **17** 033110 (2010)
205. Boyd T J M, Ondarza-Rovira R *Phys. Lett. A* **374** 1517 (2010)
206. Gonoskov A A et al. *Phys. Rev. E* **84** 046403 (2011)
207. Mikhailova J M et al. *Phys. Rev. Lett.* **109** 245005 (2012)
208. Boyd T, Ondarza-Rovira R *Phys. Rev. Lett.* **101** 125004 (2008)
209. Korzhimanov A V et al. *Phys. Usp.* **54** 9 (2011); *Usp. Fiz. Nauk* **181** 9 (2011)
210. Ma G et al. *Phys. Plasmas* **22** 033105 (2015)
211. Gordienko S, Pukhov A *Phys. Plasmas* **12** 043109 (2005)
212. Gordienko S et al. *Phys. Rev. Lett.* **93** 115002 (2004)
213. Baeva T, Gordienko S, Pukhov A *Phys. Rev. E* **74** 046404 (2006)
214. Pirozhkov A S et al. *Phys. Plasmas* **13** 013107 (2006)
215. Krainov V P, Smirnov B M, Smirnov M B *Phys. Usp.* **50** 907 (2007); *Usp. Fiz. Nauk* **177** 953 (2007)
216. Tsakiris G D et al. *New J. Phys.* **8** 19 (2006)
217. Mikhailova Yu M, Platonenko V T, Rykovanov S G *JETP Lett.* **81** 571 (2005); *Pis'ma Zh. Eksp. Teor. Fiz.* **81** 703 (2005)
218. Naumova N M et al. *Phys. Rev. Lett.* **92** 063902 (2004)
219. Naumova N M, Nees J A, Mourou G A *Phys. Plasmas* **12** 056707 (2005)
220. Edwards M R, Platonenko V T, Mikhailova J M *Opt. Lett.* **39** 6823 (2014)
221. Baeva T, Gordienko S, Pukhov A *Phys. Rev. E* **74** 065401(R) (2006)
222. Heissler P et al. *Appl. Phys. B* **101** 511 (2010)
223. Galkin A L et al. *Priklad. Fiz.* (1) 65 (2009)
224. Korobkin V V et al. *Quantum Electron.* **44** 498 (2014); *Kvantovaya Elektron.* **44** 498 (2014)
225. Seres J et al. *Nature Phys.* **6** 455 (2010)
226. Serrat C *Phys. Rev. Lett.* **111** 133902 (2013)
227. Kazamias S et al. *Nature Phys.* **6** 927 (2010)
228. Kazamias S et al. *Phys. Rev. A* **83** 063405 (2011)
229. Seres J et al. *Nature Phys.* **6** 928 (2010)
230. Strelkov V V *Phys. Rev. A* **93** 053812 (2016); arXiv:1504.07871
231. Harris S E, Sokolov A V *Phys. Rev. Lett.* **81** 2894 (1998)
232. Sokolov A V et al. *J. Mod. Opt.* **52** 285 (2005)
233. Zhi M, Sokolov A V *New J. Phys.* **10** 025032 (2008)
234. Radeonychev Y V, Polovinkin V A, Kocharovskaya O *Phys. Rev. Lett.* **105** 183902 (2010)
235. Polovinkin V A, Radeonychev Y V, Kocharovskaya O *Opt. Lett.* **36** 2296 (2011)
236. Antonov V A, Radeonychev Y V, Kocharovskaya O *Phys. Rev. Lett.* **110** 213903 (2013)
237. Vagizov F et al. *Nature* **508** 80 (2014)